A STUDY OF THE TRANSDUCTION CURRENT OF VERTEBRATE OLFACTORY NEURONS

By
Chih-Chun LIN

A dissertation submitted to Johns Hopkins University in conformity with the requirements for the degree of Doctor of Philosophy

Baltimore, Maryland
June, 2015

Abstract

Vertebrate olfactory transduction is a G-protein-coupled receptor pathway that involves the sequential activation of two ion channels to generate an electric signal in the olfactory receptor neurons (ORNs). The opening of one of these, the CNG channel, leads to Ca^{2+} influx, which then activates a calcium-activated Cl channel, Ano2 (anoctamin2 or TMEM16B). Because the chloride concentration in ORNs is constitutively high, the opening of Ano2 results in a Cl efflux, hence an inward current. Thus, the Cl current is believed to amplify the signal from the CNG channel. The CNG current in ORNs is subject to Ca^{2+}-mediated adaptation, but it is difficult to study this question in detail because the presence of the Cl current typically masks a good part of the CNG current. To understand the interaction between the CNG and Cl currents via the Ca^{2+} influx, we have succeeded in developing a method to dissect the transduction current into its CNG and Cl components, thus revealing the kinetics of each. In addition, we characterized an *Ano2*$^{-/-}$ mouse line as the platform for further study of CNG current in the future.

TABLE OF CONTENTS

TABLE OF FIGURES AND TABLES

Chapter 1

Chapter 3

Chapter 4

Chapter 5

ACKNOWLEDGEMENTS

I would like to thank members of my thesis committee, Drs. Paul Fuchs, Jeremy Nathans and Randal Reed for their constructive criticism that helped shape the thesis.

I would also like to thank Drs. Xinzhong Dong, Alex Kolodkin, David Linden and Paul Worley, with whom I did my rotations. Being naïve about neuroscience when I first joined the program, I benefited tremendously from them and established understanding across different fields in neuroscience, which eventually helped me to choose the right direction.

I would like to thank current and former lab members. Yair Ben-Chaim taught me how to do suction-pipette recording on the olfactory receptor neurons. Michael Tri Do, Donggen Luo and Tian Xue set really good examples as scientists for me to follow. Zheng Jiang and Wendy Yue joined the lab around the same time as I did and we had a great time helping each other out especially at the early phase while we are still exploring the wonders of electrophysiology. Qian Wang, Danial Silverman and Yanghui Sheng also gave useful comments to the project. Xiaozhi Ren who is the biochemistry and molecular biology expert, helped me with Western blot experiments. Rongchang Li, who joined about a year and half ago, worked with me on the project. His participation both experimentally and intellectually was indispensible for the completion of this thesis.

I especially want to thank Dr. King-Wai Yau for the opportunity to work in his laboratory. Dr. Yau is a great scientist who is willing to pass down everything he has. His passion for

science is an inspiration for me and surely for other members in the lab as well. He taught me to work with every effort instead of just ‘trying’ and always double and triple check that our results are indeed correct. All these are things I will carry on for my career.

Finally, I would like to thank my family, who gave me unconditional support throughout the years as a graduate student.

Chapter 1: Introduction

Animals rely on their sensory systems to interact with the world. Of the five senses, vision, hearing and tactile sensation each detect only a single physical modality, i.e. light, air vibration and mechanical pressure, respectively. On the other hand, taste and olfaction detect chemicals that have a vast variety of structures. While taste deals with five characters (sweet, sour, salty, bitter and umami), the olfaction sensory space has practically infinite dimensions.

1.1 Gross anatomy of olfactory system

The vertebrate olfactory system is largely conserved through evolution (Allison, 1953). The main olfactory epithelium, where the first-order olfactory neurons reside, covers part of the surface of the nasal cavity, through which the airflow occurs when an animal inhales and exhales. Bony structures called turbinates grow out from the lateral wall of the nasal cavity in reptiles and mammals, although not amphibians, producing a cavity with a convoluted bony structure (Hillenius and Ruben, 2004). This structure greatly increases the total surface area of the olfactory epithelium for capturing odorant molecules. The convoluted nasal cavity also serves to slow down the airflow, thus increasing the time during which odorants make contact with the olfactory epithelium. In mouse, the olfactory epithelium covers most of the nasal cavity (ventral 25% is covered by respiratory epithelium), but in human only the roof of the nasal cavity is covered by olfactory epithelium(Morrison and Costanzo, 1990). Mouse, but not human, has also other olfactory organs, such as vomeronasal organ and septal organ. The former is involved in detecting pheromones that have to do with reproduction or species

recognition (Boschat et al., 2002; Doving and Trotier, 1998; Hagino-Yamagishi et al., 2001; Leinders-Zufall et al., 2000; Del Punta et al., 2002; Rodriguez, 2004). The function of the latter is still unclear.

1.2 Histology of the olfactory epithelium

The main olfactory epithelium in the nasal cavity of mouse contains about ten-million olfactory receptor neurons (ORNs), the primary neurons for sensing odorants. Each ORN is bipolar in morphology, with one end being the dendrite and the other end being the axon. The tip of the dendrite is slightly enlarged, forming a structure called dendritic knob, which makes contact with the nasal mucus, and through it, the external environment. Each ORN has ~15-20 cilia emanating from the dendritic knob, thus increasing the surface area for odorant detection (Morrison and Costanzo, 1992). The axons course dorsally through the part of the cranial base called the cribriform plate, reaching the olfactory bulb. Each ORN expresses only one type of odorant receptor (Buck and Axel, 1991; Chess et al., 1994; Ngai et al., 1993; Ressler et al., 1993; Vassar et al., 1993) . Axons from ORNs expressing the same type of odorant receptor converge onto one or two glomeruli on each side of the olfactory bulb (Mombaerts et al., 1996; Ressler et al., 1993; Vassar et al., 1994), where they make contact with the dendrites of the secondary olfactory neurons called mitral cells. Convergence of these axons is believed to help increase the sensitivity of odorant detection.

1.3 Olfactory signal transduction pathway

Olfactory transduction occurs at the cilia, where the components of olfactory transduction are expressed. When an odorant binds to an OR, G_{olf} is activated, which in turn activates ACIII. The G_{olf}-ACIII complex, which is active, then elevates the cAMP concentration, which opens by direct binding a cyclic-nucleotide-gated (CNG) channel, which consists of two CNGA2, one CNGA4, and one CNGB1b subunits. The influx of Na^+ and Ca^{2+} through the CNG channel depolarizes the neuron, while Ca^{2+} also activates Ano2 to cause an additional inward current (corresponding to an efflux of Cl^-), hence further depolarizes the ORN. The ORN then fires action potentials, which are transmitted along the axon to the brain.

1.4 Brief history of the discovery of the vertebrate olfactory transduction pathway

The molecular basis of olfaction remained elusive until the mid-1980s, when biochemical evidence showed that an adenylyl cyclase that is activated by odorants is abundant in the olfactory ciliary membrane and this activation depends on the presence of GTP (Pace et al., 1985; Sklar, 1987). It was then found that pre-incubating an olfactory cilia preparations with cholera toxin would facilitate the activities of adenylyl cyclase (monitored with an assay for cAMP), thus suggesting a G_s-like G-protein being involved in the signal cascade (Pace and Lancet, 1986). Subsequent work revealed that a cyclic-nucleotide-gated (CNG) conductance similar to that found in rod and cone phototransduction is present on olfactory cilia and is activated by odorant stimulation through cAMP (Firestein and Werblin, 1989; Kurahashi, 1989, 1990; Nakamura and Gold, 1987). These components, consisting of G_{olf}, adenylyl cyclase III (ACIII) and CNG channel subunit CNGA2, were all cloned in 1989-1990 (Bakalyar and Reed, 1990;

Dhallan et al., 1990; Jones and Reed, 1989). However, CNGA2 has a $K_{1/2}$ for cAMP of ~40 μM, whereas the native CNG conductance has a $K_{1/2}$ for cAMP that is bimodally distributed at ~3 μM or ~40 μM (Nakamura and Gold, 1987). It took another 4 years before the discovery of the CNGA4 subunit, which confers the high cAMP sensitivity of the native CNG channel (Bradley et al., 1994; Liman and Buck, 1994). In fact, a third subunit, CNGB1b, consisting of an alternatively-spliced form of CNGB1 (a subunit found in the rod and cone phototransduction), is required for forming the complete native channel that is negatively regulated by Ca^{2+}-calmodulin (Bradley et al., 2004). The native channel is a heterotetramer with a ratio of 2: 1: 1 for CNGA2, A4 and B1b subunits (Bönigk et al., 1999).

All biochemical and physiological clues suggested that odorant receptors (ORs) may belong to the G-protein-coupled receptor (GPCR) family. Since the olfactory system has the ability to detect literally millions of different chemicals, it was assumed that a repertoire of many GPCRs is required. Degenerate primers targeting GPCRs were employed, and the olfactory-receptor family was cloned from a cDNA library of ORNs (Buck and Axel, 1991).

The transduction current, however, is not solely composed of the CNG current. Several studies suggested that external Ca^{2+} may play a role in olfactory transduction (Leveteau et al., 1989; Restrepo et al., 1990; Sato et al., 1991), leading to the discovery of a Ca^{2+}-activated Cl current on the plasma membrane of the olfactory cilia (Kleene and Gesteland, 1991). This Cl current was later confirmed to be activated by odorant stimulation, and

importantly, consists of an efflux of Cl^-, thus giving an inward current to depolarize ORNs like the CNG current (Kurahashi and Yau, 1993). In an odorant response, the Cl current was estimated to contribute up to ~40-85% of the total current (Kleene, 1997; Kurahashi and Yau, 1993; Lowe and Gold, 1993), and may serve to compensate for the reduced CNG current when the olfactory epithelium is exposed to fresh water (which has low external cation and low Cl^-). The finding also suggested a constitutively high Cl^- concentration in ORNs for sustaining the Cl^- efflux through open Cl channels during odorant stimulation (Kaneko et al., 2001, 2004; Nickell et al., 2007; Reisert et al., 2005). The high intracellular Cl^- concentration was found to be maintained by a Na/K/Cl cotransporter, NKCC1, although whether NKCC1 is expressed in the cilia or cell body is still under debate (Hengl et al., 2010; Jaén et al., 2011; Reisert et al., 2005). Throughout the 1990s and 2000s, many groups attempted to clone the Cl channel, and it was finally identified to be anoctomin2 (Ano2 or TMEM16B) with mass spectrometry in 2009 (Stephan et al., 2009). The story, however, did not end there. One year after the cloning of Ano2, a mouse line with Ano2 knocked out showed, surprisingly, no detectible deficit in olfactory behaviors (Billig et al., 2011). This challenges the idea that Cl current amplifies the signal in olfactory transduction.

1.5 Adaptation

Adaptation is a phenomenon found across all sensory systems. Under steady sensory stimulation, adaptation resets the sensitivity of a system so that it is able to respond to ever-stronger stimulations. In olfactory transduction, Ca^{2+}/calmodulin (Ca^{2+}/CaM) is believed to affect the signaling through 3 mechanisms. First, Ca^{2+}/CaM binds to the

CNGB1b subunit to desensitize CNG channels (Bradley et al., 2004). Second, Ca^{2+}/CaM stimulates PDE1C to facilitate the hydrolysis of cAMP (Yan et al., 1995). Third, Ca^{2+}/CaM activates CamKII, which phosphorylates ACIII to reduce its activity (Wayman et al., 1995; Wei et al., 1996). However, recent studies suggest that the significance of these mechanisms may be questionable. First of all, a mouse with the Ca^{2+}/CaM-binding domain of the CNGB1b subunit removed showed no change in sensitivity (Song et al., 2008). Another study eliminated PDE1C in mouse and demonstrated that response termination was unchanged, although sensitivity was reduced in ORNs (Cygnar and Zhao, 2009). Finally, mutating serine1076 to alanine of ACIII, therefore abolishing phosphorylation by CamKII, had no effect on the olfactory response (Cygnar et al., 2012). On the other hand, Ca^{2+}-uncaging in ORNs showed no reduction of response amplitude with repeated uncaging (Boccaccio et al., 2006). This suggests that adaptation mechanisms should be upstream of (including) the CNG channel, and Ano2 is unlikely to be involved.

1.6 Termination of olfactory response

The termination of an odorant response happens when the odorant molecule dissociates from the OR. No more G_{olf} is being activated. ACIII then stops elevating cAMP while two phosphodiesterases (PDE1C and 4A) continue to hydrolyze cAMP to 5'AMP. Lowered cAMP concentration results in CNG channel deactivation. Calcium then stops coming in through CNG channel and is being removed by a Na/Ca/K exchanger, NCKX4 (Antolin and Matthews, 2007; Reisert and Matthews, 1998; Stephan et al., 2011) and possibly diffusion of Ca^{2+} into the dendrite. The involvement of Ca^{2+}-ATPase is still

controversial. It appears to play an important role in terrestrial fire salamander (*Salamandra salamandra*), but limited in frogs (*Rana pipiens* and *Rana temporaria*), tiger salamander (*Ambystoma tigrinum*) and mouse (Antolin et al., 2010; Griff et al., 2012). Finally, Ano2 deactivates as Ca^{2+} concentration drops.

1.7 Objective of the thesis

As mentioned above, several long-accepted concepts in the olfactory transduction field are being challenged, namely, the importance of Ca^{2+}-activated Cl current and the involvement of feedback by Ca^{2+} on ACIII, PDE1C and CNG channel. It is difficult to study these issues because information on the actual contribution of Cl current to the transduction current is lacking and the kinetics of CNG current elicited by odorant is still unknown. The latter is particularly important for understanding the Ca^{2+}-mediated adaptation since CNG current should directly reflect the effect of feedback mechanisms. This dissertation, while not resolving the confusion of the field directly, aims to provide the platform for future studies. We succeeded in dissecting the transduction current into its components, CNG and Cl currents. Additionally, we characterized the 'monoclonal-nose' mouse (Fleischmann et al., 2008), which will facilitate single-cell recording from mouse ORN, and an *Ano2*$^{-/-}$ mouse line, which allows studying Ca^{2+}-mediated adaptation in the future.

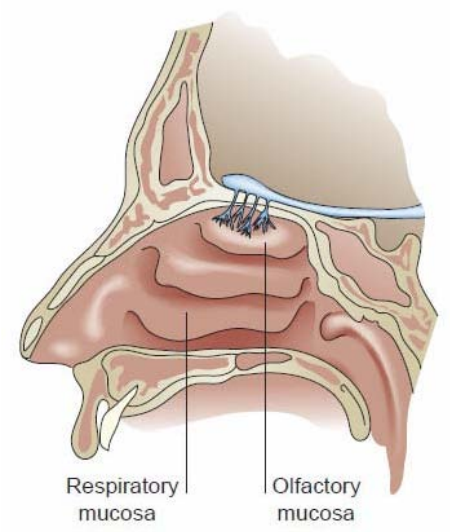

Fig. 1-1 Sagittal view of human nasal cavity.

Human nasal cavity is part of the airway. Human olfactory epithelium locates at the roof of the nasal cavity. Three bony structures, turbinates, grow into the nasal cavity from the lateral wall. In mouse, olfactory epithelium covers most part of the turbinates except for the antero-inferior part. (Adapted from Thuret et al., 2006 with permission.)

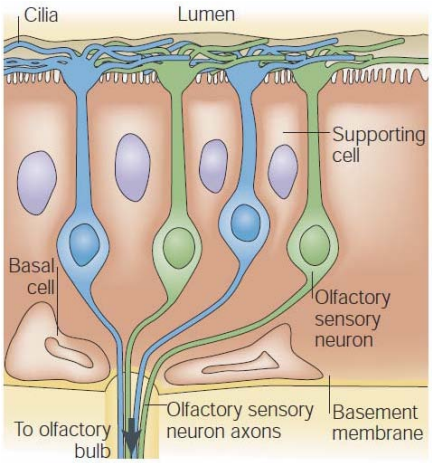

Fig. 1-2. Histology of olfactory epithelium.

Olfactory epithelium consists of three main cells types. Olfactory receptor neurons (ORNs), supporting cells and basal cells. ORNs are bipolar, with axon extending from basal aspect that course through the anterior base of the skull, forming synapse with second order neurons in the olfactory bulb. A dendrite extends apically, with an enlargement called dendritic knob on the end. About 15-20 cilia grow out from the dendritic knob and are submerged in the mucous, responsible for detecting odorant molecules. (Adapted from Mombaerts, 2004 with permission).

Chapter 2: Experimental Procedures

Tissue preparation

Rana pipiens were euthanized by pithing. Olfactory epithelium was dissected from the nose and kept in Ringer on ice. For dissociation of cells, a small piece of epithelium was laid flat with olfactory receptor neurons facing up on a Sylgard dish. Olfactory receptor neurons were released from the epithelium by gently touching the surface with a piece of razor blade, followed by several triturations. The suspension solution was placed into the recording chamber and given 30 minutes for the cells to settle down at the bottom of the chamber.

Mice between 3-6 weeks of age were euthanized followed by decapitation according to our animal protocol. The head was then cut into half along the sagittal suture and kept in Ringer on ice. When needed, olfactory epithelium (including turbinates) was dissected out and was placed in 250 μl of Ringer in a microcentrifuge tube. Brief vortex was applied and the supernatant was transferred into the recording chamber and given 30 minutes for the cells to settle down at the bottom of the chamber.

Solutions

Frog

Frog Ringer consists of NaCl 111 mM, KCl 2.5 mM, $MgCl_2$ 1.6 mM, $CaCl_2$ 1 mM, EDTA (ethlenediaminetetraacetic acid) 0.01 mM, HEPES 3 mM, glucose 10 mM, pH 7.7. Low-Ca^{2+} Ringers with Ca^{2+} concentrations of 100 nM, 10 nM, 1 nM and 0 nM were

prepared by adjusting the amount of Ca^{2+} while Mg^{2+} was increased to keep the total free divalent cation concentration constant. Low-Ca^{2+} Ringers were buffered with 1 mM EGTA (ethylene glycol tetraacetic acid) instead of 0.01 mM EDTA. Calculations were made according to MaxChelator.

Sodium chloride in Ringer was substituted with LiCl or choline chloride for Li Ringer or choline Ringer, respectively. Tetramethylammonium hydroxide was used to adjust the pH instead of sodium hydroxide.

Mouse

Mouse Ringer consists of NaCl 140 mM, KCl 5 mM, $MgCl_2$ 1 mM, $CaCl_2$ 2 mM, EDTA 0.01 mM, HEPES 10 mM, glucose 10 mM, pH 7.5. Ringer with 0-Ca^{2+} consists of NaCl 140 mM, KCl 5 mM, $MgCl_2$ 3.2 mM, $CaCl_2$ 0 mM, EGTA 1 mM, HEPES 10 mM, glucose 10 mM, pH 7.5. Sodium chloride in Ringer was substituted with LiCl or choline chloride for Li Ringer or choline Ringer, respectively. Tetramethylammonia hydroxide was used to adjust the pH instead of sodium hydroxide.

Chemicals

Odorant solution of mixture (1-heptanol, cineole, acetophenone, hexanal, (+)-citronellal), acetophenone or (+)-limonene were prepared freshly every day by diluting pure chemicals into Ringer.

Niflumic acid was prepared in two methods. One was to prepare stock solution of 150 mM niflumic acid in DMSO (dimethyl sulfoxide) and diluted to 300 μM in Ringer for experiments. A second method is directly dissolving niflumic acid into Ringer, which was heated to 37^{o}C for 1-1.5 hrs to facilitate the dissolving process.

Solution application

A motor stepper system (SF-77B, Warner Instrument) was adopted for solution application. Three manifolds each receiving 6 solution inputs are connected to a 3-barrel pipette, allowing establishment of 3 laminar flows. Flow of individual solution can be turned on and off by solenoid valves (LHDA0030300BA2, LEE). When a cell is being recorded, it is kept in the laminar flow that carries Ringer. Odorant application was carried out by having the motor stepper move the 3-barrel pipette horizontally, which allows the cell to be briefly (30 msec) exposed to laminar flow containing odorant.

Electrophysiology

An Axopatch 1C or 1D and headstage 100/1 were used for data acquisition. Signals were split into two channels and low-pass filtered through 8-pole Bessel filter of 500 Hz and 20 Hz and digitized with DigiData 1320 or 1322 at 2000 Hz. A recording pipette was pulled from standard borosilicate glass capillaries and the opening was fire polished to 4-5 μm. When the pipette is filled with Ringer, the resistance is typically 1.4 – 1.7 MΩ. During recording, the soma of an olfactory receptor neuron was drawn into the recording pipette as much as possible, while leaving the dendrite and cilia exposed to the bath. The series resistance with a cell in place is typically 8-12 MΩ.

Immunohistochemistry

Mice between 3 to 6 weeks old were anesthetized with Avertin followed by perfusion with 4% paraformaldehyde (PFA) dissolved in PBS. After fixation, the mouse was decapitated and jaw, teeth, soft palate and all soft tissue (skin, eye and fat) were removed before being kept in 4% PFA at 4^{o}C for 24 h (post-fixation). The head was washed with PBS and transferred to 30% sucrose, 250mM EDTA in PBS and kept at 4^{o}C for 24 h or longer for decalcification. The head was then embedded in tissue-freezing medium, kept at 4^{o}C for 1 h and kept on dry ice for 20-30 minutes before storage at -80^{o}C.

Coronal sections of the olfactory epithelium were cut at 14 μm thickness with a cryostat. Sections were left to dry at room temperature overnight and stored at -20^{o}C until the experiment. For immunohistochemistry, sections were fixed with 4% PFA for 5 minutes followed by three 10 minute-washes with PBS before incubation with PBS containing 0.1% Tx-100 and 5% normal goat serum (blocking solution) at room temperature for 1 h. Sections were incubated with primary antibody against Ano2 (ACL-012, Alamone Lab) in blocking solution at 4^{o}C overnight. After washing with PBS containing 0.1% Tx-100 (PBST) for 10 minutes 3 times, sections were incubated with secondary antibodies conjugated with Alexa 488 in blocking solution at room temperature for 1 h. After washing, mounting medium containing DAPI (Vectashield) was applied before coverslips were mounted. Images were taken with a Zeiss LSM 510 microscope with 10X and 20X objectives.

Western blot

Two-month-old mice were euthanized with CO_2 and perfused with PBS to remove blood. Olfactory epithelia were dissected out and placed into 8 ml ice cold Ringer and kept on ice. Calcium shock for detaching cilia was performed by adding 72 µl 1 M $CaCl_2$ to the solution, quickly mixed well on ice and placed on a rotator at 4 ^oC for 20 minutes. Solution was centrifuged at 500 RCF (relative centrifugal force) for 10 minutes at 4^oC. The pellet which contains de-ciliated epithelium was re-suspended with 600 µl denaturing buffer (DE). The supernatant which contains cilia was centrifuged again at 18500 RCF for 30 minutes at 4^oC. The pellet was re-suspended with 60 µl denaturing buffer (C). DE and C were kept in boiling water (100^oC) for 5 minutes, centrifuged at 16000 RCF for 10 minutes at room temperature. The supernatants were saved and protein concentrations were quantified with BCA (bicinchoninic acid) protein quantification assay. The concentration of DE and C were typically around 4-5 µg/µl and 0.8-1.4 µg/µl, depending on the size and age of the mice. For Western Blot, 20 µgms of protein from each sample were used for SDS-PAGE followed by transfer to PVDF membrane. The membrane was then tested with primary antibodies and visualized with ECL reagent. Primary antibodies used are G_{olf} 1:500 (Santa Cruz), ACIII 1:4000 (Santa Cruz), CNGB1b 1:10000 (gift from Martin Biel, Ludwig-Maximilians Universität München), CNGA4 1:1000 (gift from Martin Biel, Ludwig-Maximilians Universität München), PDE4A 1:500 (gift from James Cherry, Boston University), Ano2 (Almone lab, ACL-012, 1:500 and antibody against N-terminus of Ano2 from Robert Molday, University of British Columbia, Vancouver, 1:20) and M71 receptor 1:1000 (gift from Gilad Barnea, Brown University).

Chapter 3: Characterization of 'monoclonal-nose' and *Ano2*$^{-/-}$ mice

3.1 Introduction

The olfactory transduction pathway bears great similarities to the phototransduction pathway in rod and cone photoreceptors. However, olfactory transduction has not been studied quantitatively to the same depth as phototransduction for several reasons. First of all, it is difficult to apply chemical stimuli with the same temporal precision as light and the actual concentration a cell is exposed to is hard to control. This is greatly improved with the combination of a solution-change system and recording from a single dissociated ORN (see Methods). Secondly, stimuli are limited to selected concentrations prepared before experiments, unlike light, the intensity of which can be easily adjusted with appropriate filters. Finally, each ORN expresses only one out of about a thousand ORs (Buck and Axel, 1991; Chess et al., 1994; Ngai et al., 1993; Ressler et al., 1993; Vassar et al., 1993). Therefore, when performing single-cell recording, it is unlikely that randomly encountered cells would express ORs that would respond to the same prepared odorant. Even if two cells both respond to the same odorant, they are unlikely to express the same OR because one odorant can be recognized by more than one species of OR, thus making quantitative comparisons between cells impossible. This can be helped with mouse lines in which cells expressing the same OR (such as M71) are all labeled with a fluorescent protein (Bozza et al., 2002). Although one can identify in an intact epithelium those labeled cells with fluorescence optics, they are too scarce (~0.1%) to be found after dissociation (see Methods). To overcome these issues, we adopted the 'monoclonal-nose', M71-transgenic mouse line. In this mouse line, the expression of a transgenic M71 OR gene is under the control of a tet-transactivator (tTA)-responsive promoter, tet_0, and tTA

expression is under the control of OMP by having OMP-IRES-tTA knocked into the OMP locus. Since OMP is expressed in all mature ORNs, tTA is also expressed in all mature ORNs, which in turn drives the expression of M71 OR across the whole olfactory epithelium. Detailed characterization showed that ~95% of the ORNs express M71 OR (Fleischmann et al., 2008), thus it may be feasible to compare results from cell to cell.

CNG current is liable to Ca^{2+}-mediated adaptation (Bradley et al., 2004). On the other hand, it has been shown that Cl current is not involved in adaptation (Boccaccio et al., 2006). How CNG current is regulated by Ca^{2+} has not been studied in detail mainly because it is masked by Cl current. One can of course remove Cl current by removing external Ca^{2+}, but this will also remove Ca^{2+}-mediated adaptation, defeating the purpose of studying the Ca^{2+}-feedback. The calcium-activated Cl channel in the vertebrate olfactory transduction pathway is recently identified to be Ano2 (Stephan et al., 2009). *Ano2*$^{-/-}$ mouse line will be valuable for assessing the CNG current directly.

Instead of the mouse line reported (Billig et al., 2011), we obtained a mouse line in which piggyBac transposon was inserted into the 14th intron of the *Ano2*. The piggyBac transposon system was originally found in moth, *Trichoplusia ni*, and was modified to apply to mouse and other vertebrates for generating stable insertional mutagenic animals (Ding et al., 2005). The concept of the system works in the following way. Two constructs, with one containing a gene coding for the transposase, PBase, and the other containing flanking sequences that can be recognized by PBase, were injected into the pro-nucleus of a fertilized egg. The sequences recognized by PBase, along with the DNA

segment in between, were inserted into the genome by PBase. After cell division, the construct coding for PBase gene as well as its product was diluted, giving little or no PBase activity in daughter cells, therefore the inserted DNA will remain stable. Offsprings of these animals also do not express PBase, thus the animals could be bred into homozygous state without losing the insert. After characterizing this mouse line, we also crossed it with the 'monoclonal-nose' mouse line to facilitate our experiments.

3.2 Results

3.2.1 Characterization of M71-transgenic, 'monoclonal-nose', mouse (*M71*$^+$)

In *M71*$^+$ mice, the M71 OR expression is overexpressed, which may affect the expression levels of the other components of the transduction pathway and thus the physiological measurements. We thus first set out to characterize the mouse line. Western blot showed that expression levels of G_{olf}, ACIII, CNGB1b and CNGA4 were the same in *M71*$^+$ mice (Fig. 3-1). Note that only ~0.1% of wild-type ORNs express M71 OR, making it difficult to directly assess the expression level of M71 OR in wild-type mice. The expression levels of the transduction components were also assessed with mass spectrometry by measuring the mean intensity of the peak of a given protein, a surrogate index of its abundance (done by our collaborator Robert Molday). Preliminary results showed that these components are reasonably comparable in wild-type and *M71*$^+$ ORNs (Table 3-1). In terms of physiological assessment, unpublished work from our laboratory showed that the unitary response of the *M71*$^+$ ORNs was ~0.6 pA, similar to that found in wild-type ORNs. The sensitivity of *M71*$^+$ ORNs to acetophenone, a known potent ligand for M71 OR, was similar to that of M71-expressing ORNs identified genetically by eGFP (Bozza

et al., 2002 and unpublished data). Given that the expression levels of the key transduction components, the unitary response, and the sensitivity to acetophenone are all comparable to wild-type ORNs, it is likely that the expression level of M71 OR in monoclonal-nose ORNs is similar to that found in wild-type M71-expressing ORNs. The stimulus-response relation, however, should be further characterized because in those experiments the stimulus strength was changed by varying the stimulus duration instead of the odorant concentration. Varying the stimulus duration has the danger of violating the principle of impulse stimulation that we have tried to follow in our experiments.

3.2.2 Characterization of *Ano2*$^{-/-}$ mouse

It has been reported that inserting piggyBac transposon into the intron may disrupt gene splicing and gene expression (Ding et al., 2005). However, the *Ano2*$^{-/-}$ mouse line we obtained had not been characterized. We thus first tried to verify whether Ano2 expression is indeed disrupted in *Ano2*$^{-/-}$ mice. Immunohistochemistry of olfactory epithelium coronal sections from wild-type animal showed Ano2 signal in the cilia layer of the olfactory epithelium (Fig. 3-2, left) with an antibody against the 3rd putative extracellular loop of Ano2. The signal stopped at the junction between the olfactory epithelium and the respiratory epithelium (Fig. 3-2 arrow). On the other hand, tissue from *Ano2*$^{-/-}$ mice clearly showed absence of the Ano2 signal (Fig. 3-2, right). Western blot also confirmed that there is no Ano2 expression in the *Ano2*$^{-/-}$ mouse (Fig. 3-3), indicating that this mouse line is indeed an Ano2 knocked-out mouse. Heterozygous *Ano2*$^{+/-}$ animal showed decreased levels of Ano2 expression, demonstrating that protein expression parallels the number of functional allele. Since the antibody targets the 3rd

putative extracellular loop, it may still be possible that a truncated protein is made. We thus used another antibody targeting the N-terminus for Western blot, which again showed no Ano2 expression in the *Ano2*$^{-/-}$ mouse, suggesting that no truncated protein was made (Fig. 3-4). For physiological recordings, it is crucial that the expression levels of the other components of olfactory transduction are not affected as well. On Western blot, it is clear that the expression levels of G_{olf}, ACIII, CNGB1b, CNGA4, and PDE4A are the same in wild-type, *Ano2*$^{+/-}$ and *Ano2*$^{-/-}$ animals, suggesting that the expression levels of these components are independent of Ano2 expression. OMP is not part of the transduction pathway and its expression level is also unaffected (Fig. 3-3).

3.2.3 Comparing transduction current with and without Cl current

Ano2$^{-/-}$ mice were bred with M71-transgenic mice to generate *Ano2*$^{-/-}$;*M71*$^{+}$ mice. We then compared *M71*$^{+}$ ORNs with *Ano2*$^{-/-}$;*M71*$^{+}$ ORNs to reveal the role of Cl current. We studied the stimulus-response relation to acetophenone in both *M71*$^{+}$ and *Ano2*$^{-/-}$;*M71*$^{+}$ ORNs (Fig. 3-5), and the Hill coefficient and EC50 are summarized in Table 3-2. The EC50 from both *M71*$^{+}$ and *Ano2*$^{-/-}$;*M71*$^{+}$ ORNs showed a spread, which has also been found in eGFP-labeled M71-expressing ORNs (Bozza et al., 2002). However, here we showed that the spread in *M71*$^{+}$ ORNs (with Cl current present) is much larger (ranging from 17.8 to 739 μM, mean ± SD = 186.6 ± 239.2 μM) than that of *M71*$^{+}$ ORNs (ranging from 24.6 to 151μM, mean ± SD = 125.3 ± 123.7μM). Surprisingly, in both genotypes, the Hill coefficients are ~1 (*M71*$^{+}$: 1.11 ± 0.24, *Ano2*$^{-/-}$;*M71*$^{+}$: 0.81 ± 0.25). This is unexpected because both CNG channel activation by cAMP and Ano2 activation by Ca^{2+} are cooperative, which means the Hill coefficient should be greater than 1.

3.2.4 Threshold of *M71*$^{+}$ and *Ano2*$^{-/-}$;*M71*$^{+}$ ORNs

A recent study showed that *Ano2*$^{-/-}$ mice have normal olfactory behaviors (Billig et al., 2011), a surprising finding since Cl current takes up a huge portion of the transduction current (Boccaccio and Menini, 2007; Kurahashi and Yau, 1993; Lowe and Gold, 1993). We decided to approach this question by measuring the threshold for action potentials in *M71*$^{+}$ and *Ano2*$^{-/-}$;*M71*$^{+}$ ORNs.

Since impulse stimulation evokes only few spikes, averaged spike frequency and corresponding transduction current were obtained from 30 trials. The experiment was repeated at different odorant concentrations to give the relation between amplitude of transduction current and the spike frequency. Peri-stimulus spike frequency and transduction current were plotted against time in Fig. 3-6. Consistent with previous studies, action potentials only occur on the initial rising phase of a response. Firing threshold was defined as the current required for the cell to fire action potentials beyond 2 standard deviations from the baseline firing rate, a definition used in previous publication from our laboratory (Ben-Chaim et al., 2011). Six cells each were recorded from *M71*$^{+}$ and *Ano2*$^{-/-}$;*M71*$^{+}$ mice. The threshold did not differ significantly between the two genotypes (Table 3-3) and was similar to what was found in wild-type mouse ORNs ($\leq$ 2.9–4.9 pA, with mean ± SD = 3.7 ± 1.0 pA,)(Ben-Chaim et al., 2011).

Since there is no Cl current in *Ano2*$^{-/-}$;*M71*$^{+}$ ORNs, the unitary response should be smaller than the unitary response from *M71*$^{+/0}$ ORNs. Therefore, more activated receptors

are needed for achieving the threshold. It is then reasonable to arrive at the conclusion that in the *Ano2*$^{-/-}$;*M71*$^{+}$ ORN, the sensitivity is lower in terms of action-potential firing. To determine the number of activated receptors needed, it is necessary to know the size of a unitary response in the *Ano2*$^{-/-}$;*M71*$^{+}$ ORNs. This requires measuring the response in the linear range, which is too small in the *Ano2*$^{-/-}$;*M71*$^{+}$ ORNs.

3.2.5 Estimating the Ca^{2+} influx of an odorant response

Calcium dynamics is of crucial importance in olfactory transduction because it is involved in Ca^{2+}-mediated adaptation of CNG current and activates Ano2. *Ano2*$^{-/-}$ mice provides an opportunity to assess the Ca^{2+} influx during an odorant response.

To estimate the amount of Ca^{2+} in the CNG current, we substituted the external cation Na^{+} with choline and removed K^{+} and Mg^{2+}, making Ca^{2+} the only cation permeant through CNG channel. The odorant response recorded from an Ano2$^{-/-}$ olfactory receptor neuron will consist entirely of Ca^{2+} current (Fig. 3-7). Note that the junction current recorded when the cell was switched to choline Ringer was subtracted to derive the Ca^{2+}-only response. This response can be compared with a response elicited with other cations present to derive the proportion of Ca^{2+} passing through the CNG channel. However, the absence of Na^{+} in the bath will cause Ca^{2+} to accumulate in the cilia, because external Na^{+} is required for pumping out Ca^{2+} by the Na/Ca/K exchanger, NCKX4. The Ca^{2+}-mediated negative feedback will affect the response kinetics. Therefore, we performed another experiment by replacing Na^{+} with Li^{+}, which also passes through CNG channel but does not drive the exchanger, and compare this current with that obtained in choline

Ringer without K^+ and Mg^{2+}. From 3 cells, the ratio of the area under curve (total charges) from these two responses is between 30-50%. This is consistent with previous report done with heterologous expression of CNG subunits (Dzeja et al., 1999). However, it must be noted that our number is an over-estimation because of two reasons. First, Mg^{2+} competes with Ca^{2+} when passing through CNG channel, so removal of Mg^{2+} in choline Ringer results in an increase of Ca^{2+} influx (about 15% in the rod CNG channel). Second, Li^+ has been shown to pass through Na^+ better by about 10% in the rod CNG channel (Yau and Nakatani, 1984a), although data on the olfactory CNG channel is lacking. Another thing to point out is that the response of the Ca^{2+}-only current is not a simple scaling of the current elicited in Li Ringer in that the kinetics have also changed, suggesting that the proportion of transduction current carried by Ca^{2+} appears not to be constant throughout the time course of a response. Another way to measure the Ca^{2+} influx is to try to demonstrate the exchange current, similar to what had been done in the rod photoreceptors (Nakatani and Yau, 1988; Yau and Nakatani, 1984b). A response is elicited while a cell is kept in Li Ringer so NCKX4 is not functioning. When the response terminates, the cell was switched back to Na Ringer (normal Ringer) and NCKX4 resumes its function, which should result in a net inward current. However, we were unable to demonstrate this phenomenon (Fig. 4-8). It is possible that Ca^{2+} is also removed either by diffusion to dendrite/soma or the exchange current is too small to be detected (see Discussion below).

3.3 Discussion

Our biochemical results demonstrated that in *M71*$^{+}$ mice the expression levels of transduction components such as G_{olf}, ACIII, CNGB1b, CNGA4, and PDE4A are not altered by expressing M71 receptor with transgenic strategy. This allows the use of *M71*$^{+}$ mice for physiological studies with results that may be comparable to those from wild-type ORNs expressing the endogenous M71 receptor. The fact that ~95% of the ORNs express M71 receptor greatly facilitates single-cell recording. Similarly, eliminating the expression of Ano2 also had no effect on the expression levels of other key transduction proteins. Therefore *Ano2*$^{-/-}$ mouse line should provide insight into the CNG-current behavior under the regulation of different Ca^{2+}-mediated feedbacks.

The EC50 for acetophenone has a 10-fold spread in eGFP-labeled M71-expressing ORNs (Bozza et al., 2002), but we observed a near-40-fold spread of EC50 for *M71*$^{+}$ ORNs. Interestingly, *Ano2*$^{-/-}$;*M71*$^{+}$ ORNs showed only about 7-fold spread of EC50. Possibly, there is some degree of variation in M71-receptor expression among ORNs. Additionally, although the total CNG channel correlates with the amount of Ano2 on a cilium, the ratio is not exactly constant (Kleene et al., 1994). *Ano2*$^{-/-}$;*M71*$^{+}$ ORNs are subject only to expression variability of M71 but *M71*$^{+}$ ORNs are affected by the ratio of CNG channel and Ano2. The spread in eGFP-labeled M71-expressing ORNs was found with Ca^{2+} imaging (Bozza et al., 2002), therefore it only detected the signal from CNG channel. This may explain why the spread previously found is much smaller compared with our results in *M71*$^{+}$ ORNs, which include variability from both CNG and Cl channels. In fact, the spread found in *Ano2*$^{-/-}$;*M71*$^{+}$ ORNs (~7 fold), which only has CNG current, is very

close to previously reported (~10 fold). Finally, as will be shown below, the Cl current magnitude may be quite sensitive to the size of the CNG current.

There may be several possible explanations for not being able to detect exchange current. It has been suggested that Ca^{2+} is not only removed by NCKX4, but also by a Ca^{2+}-ATPase in some species (Antolin et al., 2010). Another possibility is diffusion of Ca^{2+} into the soma through dendrite, especially in a dissociated-cell preparation, might have been exaggerated by the cilia being shorter than intact ones as a result of the dissociation procedure. Calcium concentration may thus drop faster through diffusion. Shorter cilia also reduces the total number of NCKX4 available, therefore the capacity of Ca^{2+} removal by NCKX4 is compromised, making exchange current too small to be detected. The surface area of a toad rod photoreceptor is about 1000 μm^2 (diameter: 8μm, length 40 μm), which gives the maximum exchange current of a rod around 15 pA . A mouse olfactory receptor neuron has about 20 cilia, each with diameter of 0.2 μm, and length of 20 μm. The total surface area of 250 μm^2, which will give 3.5 pA of exchange current if the density of the exchanger is the same on the cilia of a mouse olfactory receptor neuron as that on a toad rod. In a cell where cilia are damaged in either length or number, the exchange current may be as low, or less than, 1 pA. Such a small exchange current may not be detectable from a dissociated mouse olfactory receptor neuron.

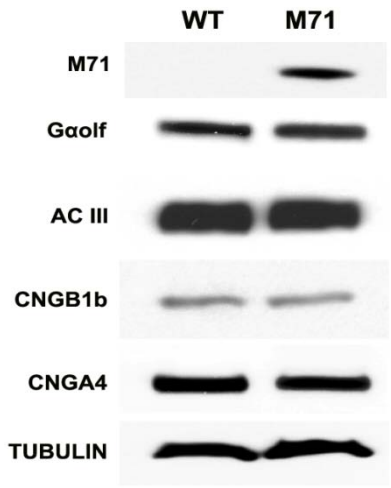

Fig. 3-1. Expression levels of selected key transduction components in *M71*$^+$ and wild-type littermates. Western blot demonstrates that the expression levels of Golf, ACIII, CNGB1b and CNGA4 are not the same between wild-type and *M71*$^+$ ORNs. Tubulin was used as loading control. M71 is detected only in *M71*$^+$ because number of ORNs expressing M71 in wild-type epithelium is ~1000 fold lower than the transgenic animal (work by Xiaozhi Ren).

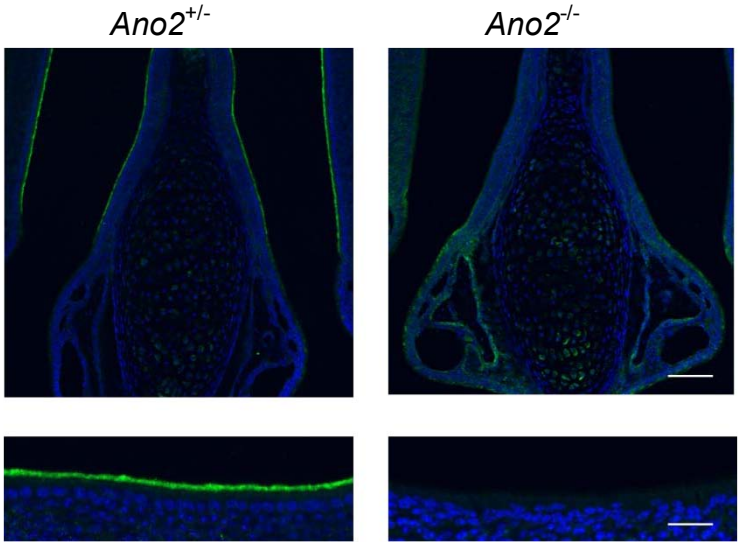

Fig. 3-2. Coronal sections of the nose from *Ano2*$^{+/-}$ and *Ano2*$^{-/-}$ mice. Upper panels, low magnification showing the nasal septum and part of two turbinates next to the septum. Ano2 is expressed only in the olfactory epithelium but not the respiratory epithelium of the *Ano2*$^{+/-}$ mouse. The junction between olfactory and respirator epithelia is marked by the arrow. Ano2 signal is absent in the Ano2$^{-/-}$, verifying the knocked-out mouse. Lower panels, higher magnification showing that the expression of Ano2 is concentrated in the cilia. Scale bars: upper panels, 100 μM, lower panels, 200 μM.

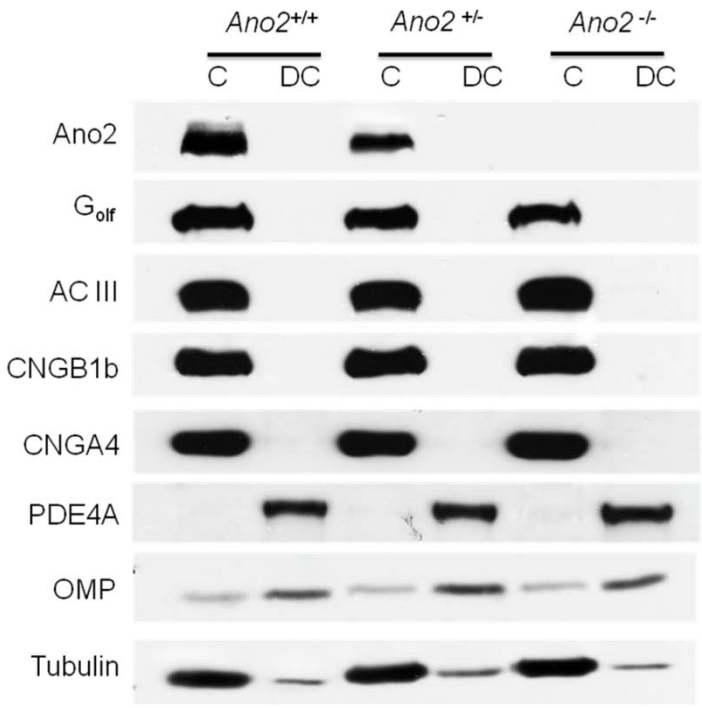

Fig. 3-3. Evaluating the expression levels of transduction components. Olfactory epithelia were collected from wild-type (*Ano2*$^{+/+}$), heterozygous (*Ano2*$^{+/-}$) and knocked-out (*Ano2*$^{-/-}$). Tissues were further separated into ciliary portion (C) and the remaining, de-ciliated epithelium (DC). Transduction components are only detected in the cilia. PDE4A is known to expression in the dendrite and cell body but not cilia, was only detected in de-ciliated epithelium. OMP was detected in both cilia and de-ciliated epithelium. Tubulin was used as loading control. Ano2 expression decreases in Ano2$^{+/-}$ and absent in Ano2$^{-/-}$. Expression levels of other proteins are unchanged across all genotypes. 20 μg of protein were loaded for each lane (work by Xiaozhi Ren).

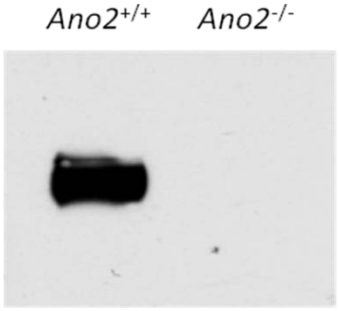

Fig. 3-4. Western blot probed with antibody against N-terminus of Ano2. Ciliary protein of 20 μg from *Ano2*$^{+/+}$ and *Ano2*$^{-/-}$ was loaded to each lane and blotted with antibody against N-terminus of Ano2. No Ano2 was detected in the Ano2$^{-/-}$, confirming no truncated protein was made (work by Xiaozhi Ren).

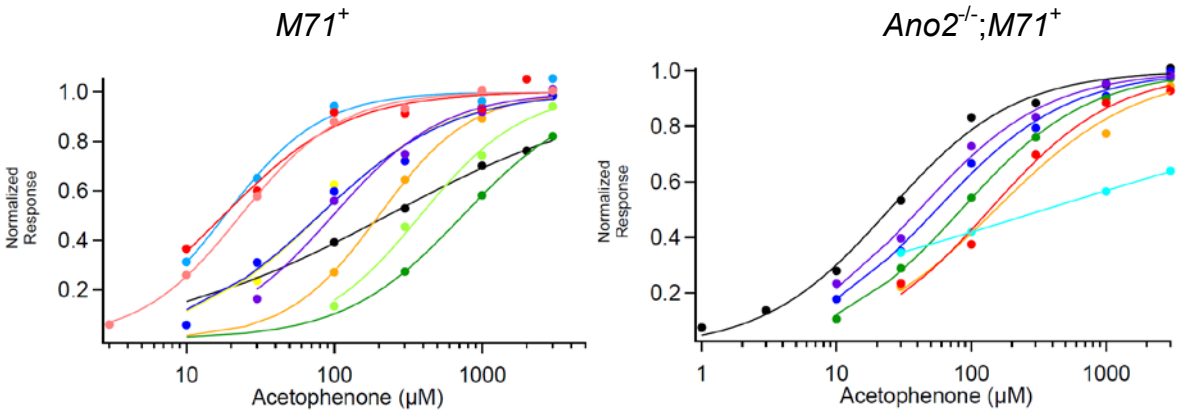

Fig. 3-5. Dose response curves of *M71*$^{+}$ and *Ano2*$^{-/-}$;*M71*$^{+}$ ORNs. Collected data of 10 cells from *M71*$^{+}$ and 7 cells from *Ano2*$^{-/-}$;*M71*$^{+}$ are shown. The Hill coefficients are around 1.11±0.24 for *M71*$^{+}$ and 0.81±0.25 for *Ano2*$^{-/-}$;*M71*$^{+}$ ORNs (see Table 3-2 for results of individual ORN). In each genotype, there is an outlier, black in *M71*$^{+}$ and light blue in *Ano2*$^{-/-}$;*M71*$^{+}$. The transgenic line have ~95% of the ORNs expressing M71 receptor but still have ~5% of the ORNs expressing one out of the other receptor species. It is likely the two cells do not express M71 receptor.

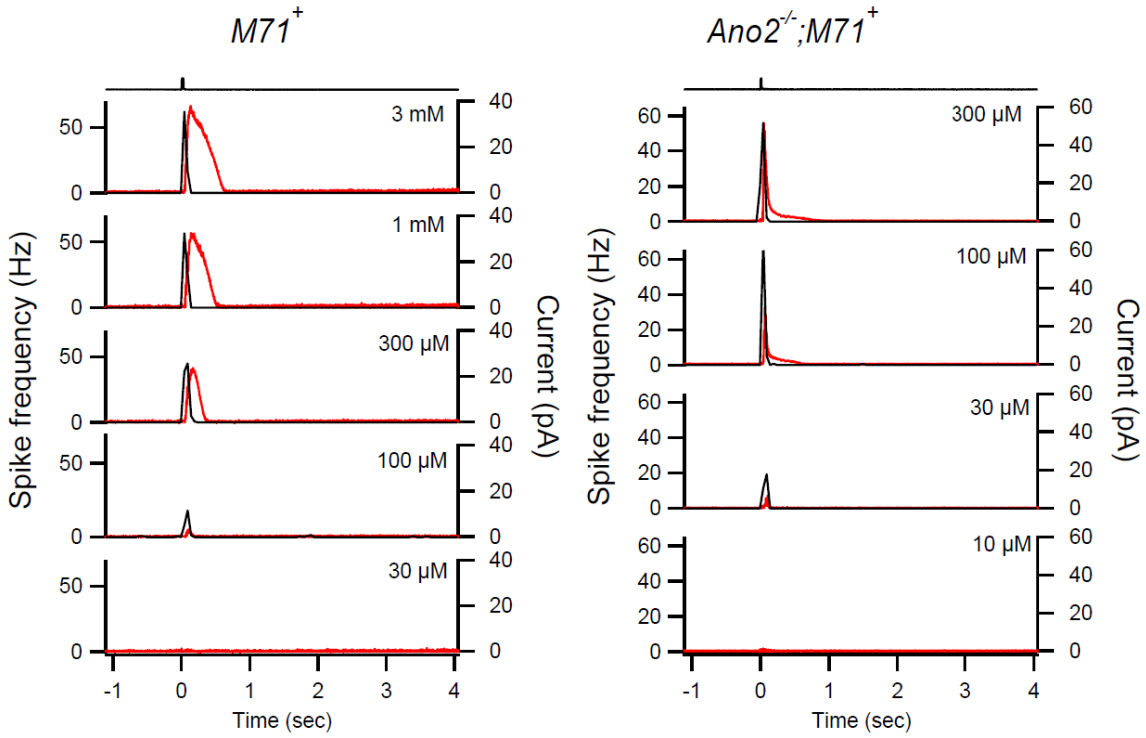

Fig. 3-6. Threshold of *M71*$^{+}$ and *Ano2*$^{-/-}$*;M71*$^{+}$ ORNs. A 30 msec pulse of acetophenone was used to stimulate the ORNs repeatedly for 30 trials. Families of instantaneous spike frequency from two representative ORNs (black traces) are plotted against time. Concentrations used are marked on the upper right of each panel. Corresponding transduction currents are plotted in red. Threshold was defined as the transduction current required to generate spike frequency two standard deviations higher than the baseline firing rate. Because we can only prepare limited number of concentrations for each experiment, the current recorded in each cell that reached threshold will be higher than the minimal current needed. For the ORNs in the figure, the threshold is ≤ 3.17 pA for *M71*$^{+}$ ORN and ≤ 5.13 pA for *Ano2*$^{-/-}$*;M71*$^{+}$ ORNs (please see Table. 3-3 for data from individual ORNs). Timing of the odorant stimulation is illustrated at the top of each family.

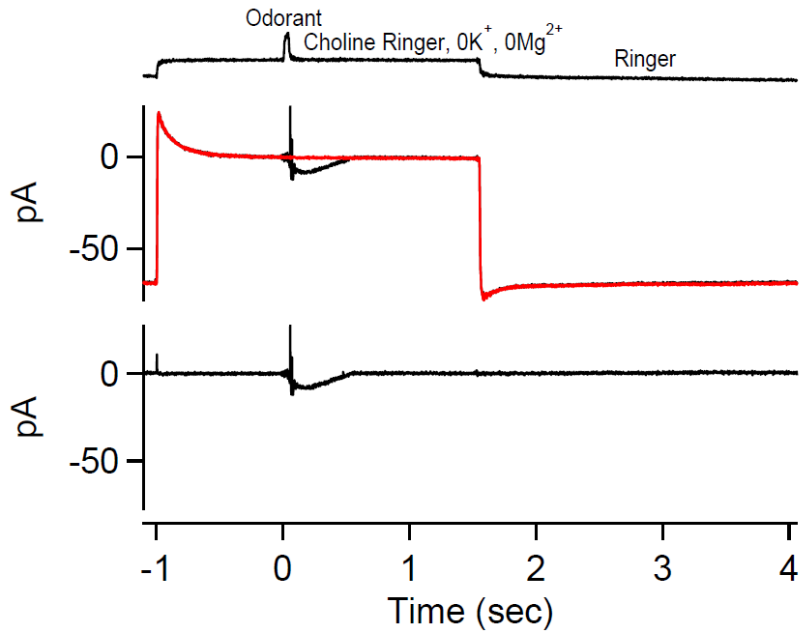

Fig. 3-7. Response in choline Ringer with 0 K^+ and 0 Mg^{2+}. The ORN was kept in choline Ringer for 1 sec before a 30 msec pulse of odorant was applied. Upper panel, raw traces showing that when switching external solution to choline Ringer, a junction current developed. Junction current (red) was subtracted from the trace with odorant stimulation (black) in the upper panel to give the trace at lower panel. Notice that a small artifact can be seen at the timing of solution change in the lower panel due to slight inconsistency of the junction current.

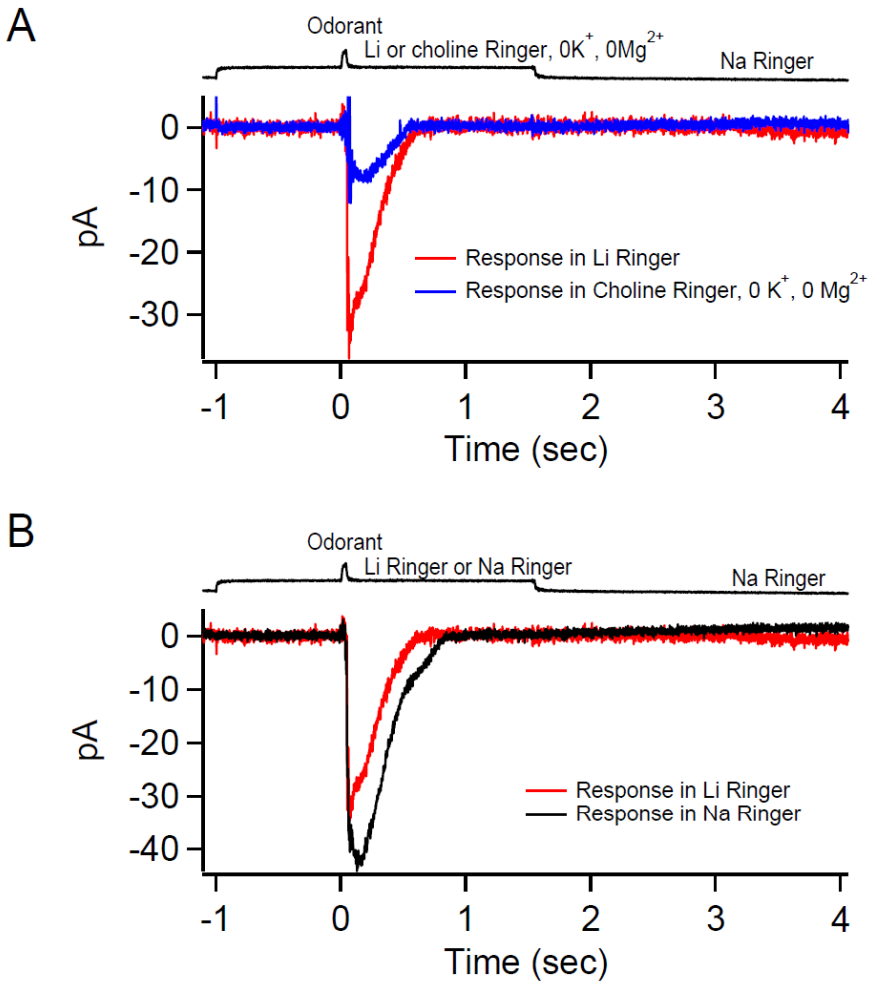

Fig. 3-8. Estimating Ca^{2+} influx in a response. A. Odorant responses in choline Ringer with 0 K^+ and 0 Mg^{2+} and Li Ringer were compared. Response in choline Ringer with no other permeant cation should give rise to pure Ca^{2+} current. Response in Li Ringer, however, consists of Li^+, Mg^{2+} and Ca^{2+}. Comparing between the two provide estimation of the amount of Ca^{2+} passing through CNG channel in an odorant response. One should compare these two instead of comparing response in choline or Li to response in Na Ringer, because the Na/K/Ca exchanger is not driven by choline or Li, therefore Ca^{2+} may accumulate in the cilia, resulting in stronger negative feedback and speed up the CNG current termination. This can be demonstrated in **B**, which compares responses from Li and Na Ringer.

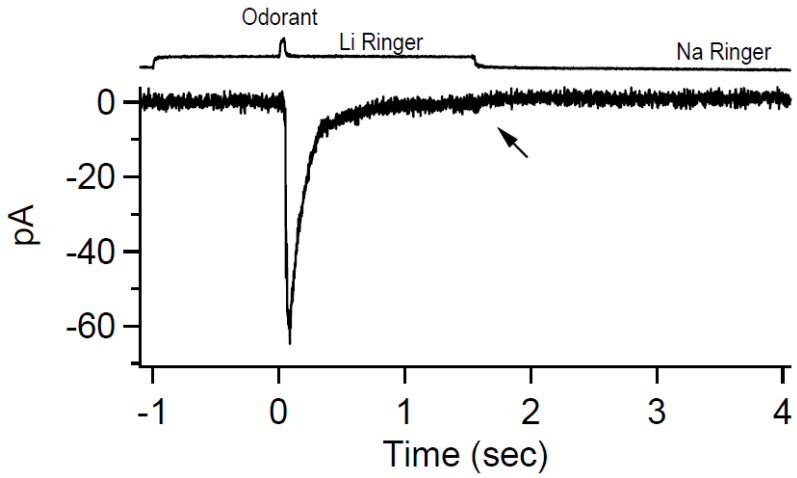

Fig. 3-9. Attempt to measure exchange current. An odorant response from *Ano2*$^{-/-}$ ORN was elicited in Li Ringer and switched back to Na Ringer. Because Li Ringer cannot drive Na/K/Ca exchanger, Ca^{2+} is expected to be trapped inside cilia. Upon switching back to Na Ringer (arrow), the exchanger should start again, generating an exchange current. However, no obvious exchange current was observed.

Wild-type Olfactory Cilia				*M71*$^{+}$ Olfactory Cilia			
Protein	% Peptide Coverage	Mean Intensity	Ratio	Protein	% Peptide Coverage	Mean Intensity	Ratio
M71 OR	-------	---------	-------	M71	9.3	1,960,000	0.17
Gα(olf)	51.5	15,200,000	1	Gα(olf)	62.4	11,500,000	1
Gβ(olf)	66.1	2,420,000	0.16	Gβ(olf)	68.2	2,800,000	0.24
ACIII	43.8	780,000	0.051	ACIII	41	940,000	0.082
CNGA2	29.9	1,850,000	0.12	CNGA2	28.7	1,960,000	0.17
CNGA4	23.8	2,770,000	0.18	CNGA4	23.1	3,060,000	0.27
CNGB1b	28.8	1,850,000	0.12	CNGB1b	24.2	1,840,000	0.16
PDE1C	50.0	2,040,000	0.13	PDE1C	49.2	1,490,000	0.13
ANO2	36.7	2,120,000	0.14	ANO2	38.2	1,880,000	0.16

Table 3-1. Mass spectrometry data from purified cilia of wild-type and *M71*$^{+}$ mice.

The relative abundance of each protein correlates with the ratio, which was normalized to the amount of α subunit of G_{olf}.

M71^{+}

Cell	Hill Coeffecient	EC50 (μM)
1	1.05	17.82
2	0.55	229.05
3	0.99	80.05
4	1.4	200.07
5	0.97	79.01
6	1.08	739.28
7	1.34	18.21
8	1.16	97.77
9	1.28	23.21
10	1.25	381.65
Mean	1.107	186.61
S.D.	0.24	226.04

Ano2$^{-/-}$; *M71*$^{+}$

Cell	Hill Coeffecient	EC50 (μM)
1	0.93	24.63
2	0.89	55.17
3	0.92	84.18
4	0.83	150.99
5	0.93	137.07
6	0.91	41.05
7	0.26	384.57
Mean	0.81	125.38
S.D.	0.24	123.74

Table 3-2. Hill coefficient and EC50 from *M71*$^{+}$ and *Ano2*$^{-/-}$;*M71*$^{+}$ ORNs.

Two ORNs from each genotype showed unusually low Hill coefficient (marked red).

EC50 showed wide spread in both genotypes, especially from *M71*$^{+}$ ORNs.

	M71^{+}	*Ano2*$^{-/-}$;*M71*$^{+}$
	Amplitude(pA)	Amplitude(pA)
	2.39	1.73
	2.40	4.06
	2.96	5.13
	3.17	5.79
	1.27	2.29
	2.69	2.63
Mean	2.48	3.61
SD	0.67	1.64

Table. 3-3. Transduction current required to reach firing threshold in *M71*$^{+}$ and *Ano2*$^{-/-}$;*M71*$^{+}$ ORNs. The currents required are not significantly different from each genotype.

Chapter 4: Dissection of olfactory transduction current

4.1 Introduction

Chloride current has been estimated to take up to 90% of an odorant response, therefore believed to provide a non-linear amplification to the signal generated by CNG current. One commonly adopted approach to separate CNG and Cl current is voltage-clamping the cell at the Cl reversal potential. However, dialysis by pipette solution rendered the intracellular Cl^- concentration artificial. To solve this problem, some have tried perforated patch with gramicidin, which is impermeable to Cl^-. Even though the native Cl^- concentration is preserved, voltage-clamping will change the electrochemical driving force, therefore one may get an artificially large Cl chloride current (Lowe and Gold, 1991). Therefore, a precise study of the CNG and Cl current magnitude and kinetics has never been obtained. Although *Ano2*$^{-/-}$ mouse are now available, which can provide information of the CNG current kinetics and lend access to understanding the Ca^{2+} regulation, it is not legitimate to compare the current recorded from wild-type cells versus *Ano2*$^{-/-}$ cells. The main reason is that each cell may have different maximal current and sensitivity, even if they express the same odorant receptor (see Chapter 3). Thus simply comparing the response of a wild-type neuron to that of an *Ano2*$^{-/-}$ neuron does not give information of how much Cl current is in an odorant response from a wild-type cell. To make the comparison, one has to compare the response with and without Cl current in the same cell. We therefore decided to pursue the question with pharmacology.

Niflumic acid has been widely employed in studying the Ca^{2+}-activated Cl current in olfactory receptor neurons (Boccaccio and Menini, 2007; Kleene, 1993; Lowe and Gold,

1993; Reisert et al., 2005). It has been demonstrated that 300 μM niflumic acid blocks > 90% of the Ca^{2+}-activated Cl current in excised cilia from *Rana pipiens*, while having no effect on the amplitude of CNG current (Kleene, 1993). However, a recently published work showed that niflumic acid reduced the electro-olfactogram (EOG) response from olfactory epithelium of *Ano2*$^{-/-}$ mice (Billig et al., 2011), which should only consist of CNG current, suggesting niflumic acid may not be as specific as previously claimed. To adopt niflumic acid for our own study, we first set out to re-examine the properties of niflumic acid.

4.2 Results

4.2.1 Effect of niflumic acid on transduction current

As expected, when a wild-type mouse ORN was briefly (150 msec) exposed to niflumic acid after odorant stimulation, but while an odorant-induced transduction current was ongoing, the current was inhibited because niflumic acid blocks Ano2 (Fig. 4-1, upper left panel). When the same experiment was repeated in *Ano2*$^{-/-}$ ORNs, in which odorant stimulation elicits pure CNG current, there is no inhibition by niflumic acid (Fig. 4-1, upper right panel). In wild-type ORNs, pure CNG current also can be elicited if the cell is kept in 0-Ca^{2+} Ringer. We therefore performed the same experiment on both wild-type and *Ano2*$^{-/-}$ ORNs. Again, niflumic acid does not inhibit the transduction current when there is only a CNG component (Fig. 4-1, lower two panels). However, when niflumic acid was applied to an *Ano2*$^{-/-}$ ORN before and during, instead of after, the odorant stimulation, the response was reduced (Fig. 4-2). These results suggested that niflumic acid does not itself block the CNG channel. It may, however, affect the signal

transduction pathway upstream of the CNG channel opening, e.g. odorant-receptor interaction, therefore reducing the amplitude of the CNG current. In other words, niflumic acid is indeed a specific blocker for Ano2, consistent with the results from *Rana pipiens* (Kleene, 1993). This also explains why, in the more recent report, the authors observed reduction of CNG current in EOG experiments done on *Ano2*$^{-/-}$ mouse (Billig et al., 2011). In their experiment, niflumic acid was in the bath before, during and after odorant stimulation, therefore the result is the combination of all three scenarios described above.

4.2.2 Niflumic acid inhibition is not instantaneous

Niflumic acid was applied to a *M71*$^{+}$ ORN during two odorant responses, with the timing of niflumic-acid application delayed for 60 msec in the second trace (Fig.4-3A, blue trace). Upon exposure to niflumic acid, the current first demonstrated a sharp decline, followed by a much slower second phase, during which the red and blue traces overlap with each other (Fig.4-3A, arrow marks the time two traces first overlap). This indicates niflumic acid has reached a steady state during the time of overlap. By applying niflumic acid pulses each delaying for 60 msec to repeatedly elicited odorant responses, we can obtain an envelope of overlapping segments, which represents the time course of the current that is not blocked by niflumic acid to estimate the CNG current in a response. However, looking at the blue trace, it takes ~65 msec from the beginning of niflumic acid exposure (Fig.4-3A, blue dashed line) to reach the steady phase (Fig.4-3A, arrow). Therefore, even if we applied niflumic acid right after the odorant stimulation, there will still be about ~60 msec dead time (Fig. 4-3B, shaded area), where the exact degree of

inhibition is unknown. This rendered current separation at the rising phase and the peak of a mouse ORN response impossible. Incidentally, the response from a frog (*Rana pipiens*) ORN has a significant delay between the application of odorant and the onset of the response (Fig. 4-4, lower panel), which is not present in the mouse (Fig. 4-4, upper panel). The dead time of the niflumic acid effect in frog ORNs is not delayed compared with that in the mouse ORN (Fig. 4-5). Importantly, in frog ORNs, two traces with niflumic acid given 60 msec apart still overlap (Fig. 4-5), similar to that found in mouse ORNs. These allow us to adopt niflumic acid to dissect the transduction current through the entire time course in a frog ORN.

4.2.3 Complication of long exposure to niflumic acid

When the cell was given a long pulse (500 msec) of niflumic acid, the residual current became smaller compared with the residual current of another pulse that was delayed for 250 msec (Fig. 4-6). This complication will be explained further in a later section (see current rebound after removal of niflumic acid) and it can be avoided if niflumic acid is given with pulses that are spaced apart by 60 msec, for which the residual currents will overlap, as described earlier (Fig. 4-3 and Fig. 4-5).

4.2.4 Effect of DMSO

The solubility of niflumic acid in Ringer is low (250 mg/l at pH. 6.2, Bres et al., 1976), so it is typically prepared as concentrated stock in DMSO at 150 mM and diluted to 300 μM in Ringer when used (DMSO final concentration is 0.2%). However, when performing experiments with frog ORNs, we noticed that DMSO itself may give rise to an odorant

response (Fig. 4-7A, left panel). Although rare, we observed such a response in one out of 34 cells (Fig. 4-7B). In addition, even when DMSO did not elicit a response, it will cause an artifact in about 47% (16 out of 34) of the cells (Fig. 4-7B). The artifact usually manifests as an inward current which does not share the same kinetics as a real odorant response (Fig. 4-7A, left panel). This artifact should not be confused with an odorant response. In fact, the illustrated DMSO-induced odorant response also shows a similar artifact before the actual odorant response rises (Fig. 4-7A left panel). To avoid this artifact and the rare chance of encountering a DMSO-responding ORN, we decided to directly dissolve niflumic acid in Ringer for our experiments. The inhibitory effect of niflumic acid with and without DMSO does not differ significantly (Fig. 4-8). However, before we realized DMSO may introduce this confounding factor, some experiments were performed with the presence of DMSO. In these experiments, only cells that had neither odorant responses to DMSO nor artifact were included.

4.2.5 Effect of niflumic acid alone

In contrast to DMSO, niflumic acid alone produced artifacts less frequently (13%, 5 out of 39 cells, Fig. 4-7 B). The artifact looks similar to that caused by DMSO (Fig. 4-7 A right panel). In one out of 39 cells, we recorded a true odorant response to niflumic acid. However, more frequently we saw a short train of action potentials (1-4 spikes) without an apparent transduction current (Fig. 4-7 A right panel). The fact that action potentials were generated suggests there is still a depolarizing current that is below our detection level.

4.2.6 Niflumic acid effect on CNG current is similar in frog

To make sure niflumic acid does not affect CNG current in frog, we repeated the experiments in Fig. 4-1 and Fig. 4-2. *Ano2*$^{-/-}$ frogs are not available, so the experiments were done in 0-Ca^{2+}-Ringer to make odorant-induced current carried purely by CNG channel. Consistent with the results in mouse, niflumic acid also does not inhibit CNG current in frog once CNG channels are activated, but it affects the upstream transduction pathways when applied before or during odorant stimulation (Fig. 4-9).

4.2.7 Current rebound after removal of niflumic acid

Upon removal of niflumic acid pulse, the transduction current may show a rebound (Fig. 4-10A). This phenomenon has been described but had not been studied further (Lowe and Gold, 1993). To assess the nature of this rebound current, a second niflumic acid pulse was applied during the rebound current and demonstrated strong inhibition (Fig. 4-10B), suggesting the rebound current is mostly composed of Cl current. The magnitude of the rebound (the difference between the rebound and the control) goes down as the transduction current approaches saturation (Fig. 4-11). This phenomenon can be accounted for if niflumic acid causes a small increase of intra-ciliary Ca^{2+} concentration. In this context, the size of the rebound will be affected by the intra-ciliary Ca^{2+} concentration when niflumic acid is applied. One can imagine that along with the Ano2 activation dose-response, the same amount of Ca^{2+} increase results in smaller increase of Ano2 current when the Ca^{2+} concentration is near-saturation Cl current (Fig. 4-12). The Ca^{2+} increase introduced by niflumic acid should be very small because when niflumic acid was applied alone, we never saw an obvious current. However, we typically

observed action potentials, suggesting that niflumic acid can induce a depolarizing current that is below the detection level, but can still reach the firing threshold. A small increase in intra-ciliary Ca^{2+} also explains what we saw in Fig. 4-6, where longer exposure to niflumic acid resulted in reduction of the residual current. This is because the additional Ca^{2+} negatively feeds back onto CNG channel. Using niflumic acid pulses that are spaced only by 60 msec can minimize this unwanted effect so that it does not interfere with our experiments, as illustrated in Fig. 4-3 and Fig. 4-5. We thus attempted to separate CNG current from Cl current with the following method.

4.2.8 Dissecting the transduction current

A series of 150 msec niflumic acid pulses each delayed by 60 msec was given during an odorant response (Fig. 4-13). We connected the overlapping residual current segments and obtained the envelope of the residual current through the whole time course (highlighted red in Fig. 4-13 lower panel). Similar experiments had been executed by Lowe and Gold with whole cell recording of rat olfactory receptor neurons, although a continuous envelope was not available because their series of niflumic acid application did not have overlapped timing. The time course of residual current parallels that of the total current (Fig. 4-14 A), which is consistent with Lowe and Gold's finding. We divided the residual current by the total current to reveal the change of the fraction of the total current being residual current through time. Interestingly, this fraction became constant at the tail of an odorant response (Fig. 4-14 B, 0.23 in this case), which lead to the following thoughts.

Niflumic acid has been reported to inhibit more than 90% of the Cl current at 300 μM (Kleene, 1993), therefore it is widely used for estimating the CNG current of an odorant response. If indeed niflumic acid blocks more than 90% of the Cl current, the residual current should mostly be CNG current. The fixed fraction would suggest that CNG and Cl currents were maintained at a constant ratio, or that Cl current is 'linearly' amplifying CNG current. This is unlikely since activation of Ano2 by Ca^{2+} has a Hill coefficient that is greater than 1, which is 'non-linear' (Kleene, 1993).

An alternative explanation is that the tail of the residual current consists of only Cl current, and the residual current simply reflects the Cl current that is not blocked by niflumic acid. In fact, recent reports have showed that the inhibitory effect of niflumic acid ranges from 47% to 87% instead of > 90% (Huang et al., 2012; Reisert et al., 2003; Sagheddu et al., 2010a; Stephan et al., 2009), consistent with our hypothesis.

4.2.9 Tail of an odorant response has little or no CNG current

To investigate whether the tail of an odorant response indeed is composed of Cl current only, we substituted Na^+ in the bath with $choline^+$. If the current has both CNG and Cl components, then when the cell is kept in choline Ringer, one will observe a reduction of the current because choline is not permeant through CNG channel. If only Cl current is present, then switching to choline Ringer will not change the current amplitude. However, since choline does not drive NCKX4, Ca^{2+} will accumulate in the cilia and slow down the relaxation of Cl current. Therefore, we also recorded the response in Li Ringer (Li^+ also does not drive the exchanger, but passes through the CNG channel similarly to Na^+, if not

slightly better) (Yau and Nakatani, 1984a). When solution change was performed at an earlier time point of a response, one can see that the current becomes smaller in choline Ringer compared with the current in Li Ringer (Fig. 4-14 C top panel). However, when solution change was done at the later part of a response, the current remained the same in both choline and Li Ringer, followed by identical relaxation (Fig. 4-14 C middle and lower panels). This supports the idea that CNG current terminates early in an odorant response and the tail of a response consists of Cl current only, as concluded previously (Reisert and Matthews, 1998). In summary, niflumic acid does not block all Cl current, so the residual current is a combination of CNG current and a fraction of Cl current. Since CNG current terminates early, the tail of the residual current is entirely composed of Cl current. The fixed fraction X, 0.23 in the cell illustrated in Fig. 4-14, at the tail of a response thus gives the fraction of Cl current spared by niflumic acid.

4.2.10 Dissecting the transduction current

We can then derive the total Cl current by scaling the blocked Cl current (difference between total current and residual current) with factor (1-X) (0.23for this cell). The CNG current is then derived by subtracting Cl current from total current. Applying this method to the family of traces recorded from a cell gives the family of dissected CNG and Cl currents (Fig. 4-15A). For all the responses in the family, the majority of the total current consists of Cl current. In fact, for the lowest two responses there is barely detectable CNG current, even though the total current is ~40 pA. This demonstrates that only little Ca^{2+} is required for generating a huge Cl current, consistent with the idea that Cl current non-linearly amplifies CNG current. The same method can also be applied to a mouse

ORN which shows similar results (Fig. 4-16), although one should remember that there is a delay of niflumic acid action, making the dissection at the rising phase and peak of the responses inaccurate. This frog cell has not reached saturation even with 10 mM of (+)-limonene (Fig. 4-15B).

Another cell in which the response reached saturation is shown in Fig. 4-17, again indicating that Cl current takes up the majority of the total current. One can appreciate that Cl current becomes saturated earlier than the CNG current, whereas the CNG current amplitude continues to increase with stronger stimuli. Additionally, the time-to-peak of Cl current is longer than that of CNG current. Therefore at weak stimuli, where the CNG current is very small, the time-to-peak of the total current is dominated by the time-to-peak of Cl current. As the stimulus strength increases, the time-to-peak of the total current shifts earlier as the peak of CNG current takes over. Plotting the peak amplitudes of Cl/CNG currents versus stimulus concentration (Fig. 4-17D) also demonstrates that amplification by Cl current is decreased as stimulation strength is increased.

4.3 Discussion

We carried out a detailed characterization of action of niflumic acid on the olfactory transduction response and provided detail explanation of its complication. First of all, it is clear that niflumic acid is a specific inhibitor of Ano2. It does not directly block CNG channels, however, it may interact with the transduction steps upstream of CNG activation. Therefore the timing of niflumic acid application is crucial when using the blocker.

Secondly, apart from inhibiting Cl channels, it appears to introduce a small rise of intra-ciliary Ca^{2+} concentration. The source of the Ca^{2+} rise is still unclear. It has been suggested that niflumic acid can induce Ca^{2+} release from endoplasmic reticulum (ER) (Kucherenko and Lang, 2014). Although ER does not extend into cilia, it may still be possible that Ca^{2+} is released in the soma or dendrite and diffuses into the cilia. Niflumic acid is known to activate TRPA1 (Hu et al., 2010), which is expressed in ORNs (Nakashimo et al., 2010) and is a non-selective cation channel. In any case, it is clear that the amount of Ca^{2+} increase caused by niflumic acid is very small since no current is observed when niflumic acid is applied alone.

We also demonstrated that CNG current actually terminates early and the tail of an odorant response is basically Cl current alone. It should be noted that our detection resolution is around 1 pA. It is possible that, in the Li/choline solution exchange experiment, some remaining CNG current that is below detection level may still exist. However, this will not affect our method to dissect the CNG and Cl current.

We have, for the first time, achieved dissection of the transduction current into its components without clamping the membrane potential or dialyzing the intracellular ion concentrations or Ca^{2+} buffering. We can therefore examine the kinetics of the two currents in physiological conditions. It has been reported that Cl current rises more slowly than CNG current in whole-cell recording (Boccaccio and Menini, 2007). We also observed a similar finding although not as pronounced. In fact, the total transduction

current in the previous report showed a multi-phasic rise (Boccaccio and Menini, 2007), that was not observed in our recordings. It is likely that intra-cellular Ca^{2+} buffering was altered by dialysis during whole-cell recording delaying the rise of intra-ciliary Ca^{2+}.

It is known that the spike train is mostly at the beginning of an odorant response. Here we demonstrated that the rising phase of a response is mostly CNG current, while Cl current, being delayed compared with CNG current, has little if any contribution to the rising phase. This suggests that Cl current may not be involved in the generation of action potentials, which is consistent with the idea that Cl current may be dispensable in olfactory transduction in mouse (Billig et al., 2011). However, Cl current still depolarizes the cells, therefore may still affect action potential firing if a second stimulus immediately follows the first response. At this point, it is still unclear what the real role of Cl current is.

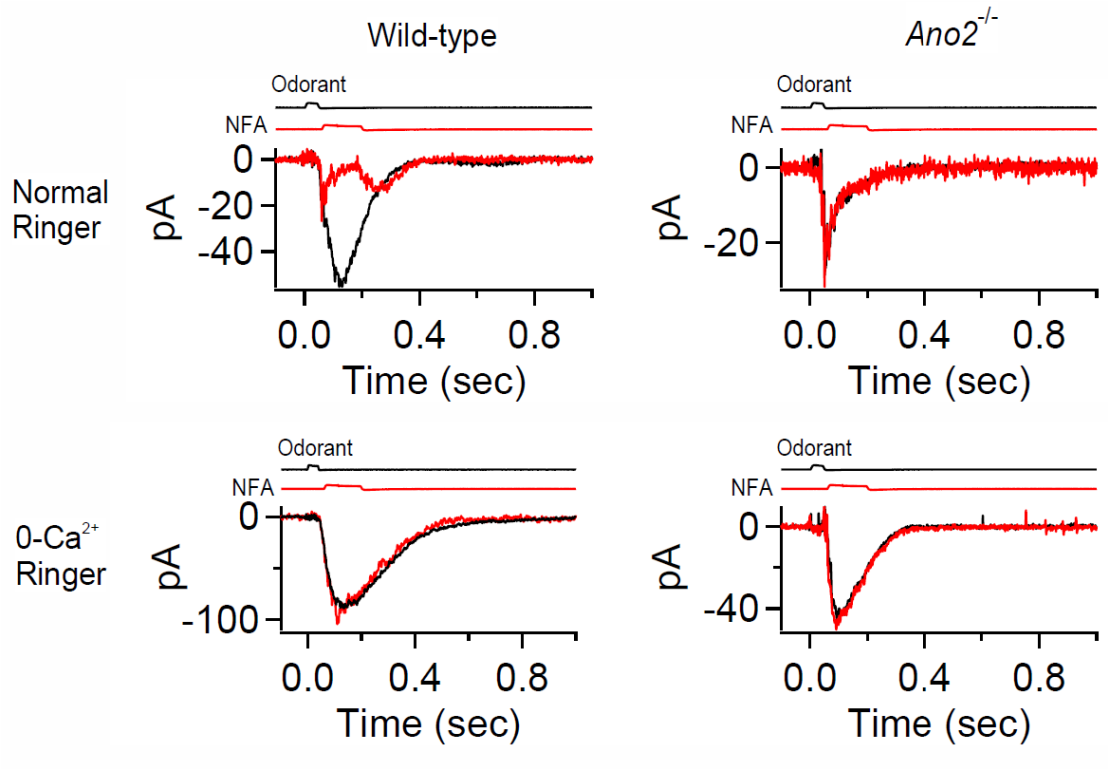

Fig. 4-1. Niflumic acid inhibits Cl current but not CNG current.

Upper left, 40 msec of 300 μM odorant mixture elicited an odorant response in a wild-type mouse ORN in normal Ringer solution (black trace). The response can be inhibited by 150 msec exposure to 300 μM niflumic acid, when it is applied during the response (red trace). **Lower left**, response from same wild-type ORN in 0-Ca^{2+} Ringer (black trace) is not inhibited by niflumic acid (red trace). **Right**, responses from an *Ano2*$^{-/-}$ ORN in normal Ringer (upper) and 0-Ca^{2+} Ringer were not affected by application of niflumic acid if it is given after odorant was applied. Timing of odorant or niflumic acid application is indicated above each panel by junction current measured with 90% Ringer. NFA: niflumic acid. Odorant: mixture of 300 μM of each of the following chemicals: 1-heptanol, cineole, acetophenone, hexanal, (+)-citronellal.

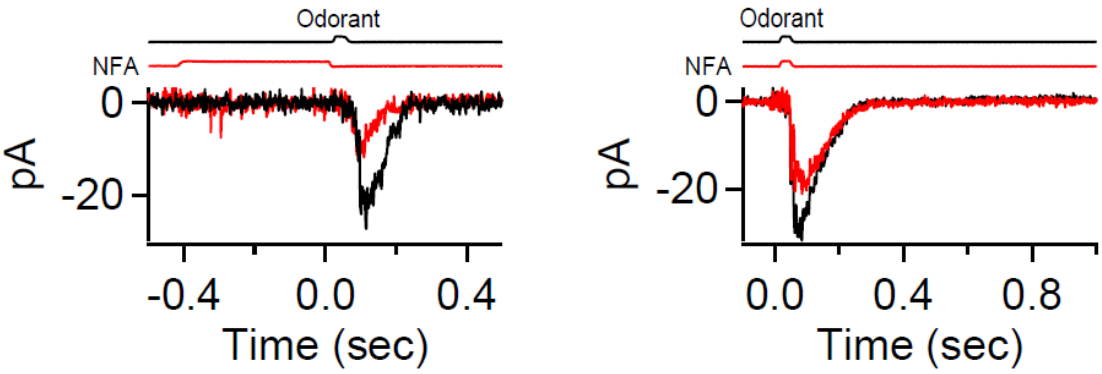

Fig. 4-2. Niflumic acid may affect CNG current if applied before or during odorant pulse. Responses to 40 msec 300 μM odorant mixture from an *Ano2*$^{-/-}$ mouse ORN (black traces). **Left**, 300 μM niflumic acid was given for 400 msec immediately before odorant pulse was given attenuated the odorant response (red). **Right**, when niflumic acid was given simultaneously with the odorant, response is also reduced. Timing of odorant or niflumic acid application is indicated above each panel by junction current measured with 90% Ringer. NFA: niflumic acid. Odorant: mixture of 300 μM of each of the following chemicals: 1-heptanol, cineole, acetophenone, hexanal, (+)-citronellal.

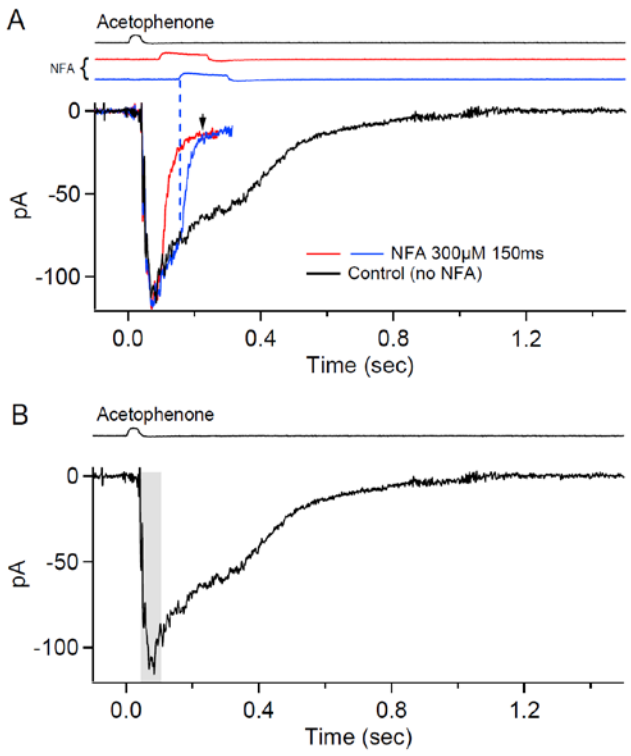

Fig. 4-3. Niflumic acid effect is delayed.

A, 300 µM acetophenone results in an odorant response from a *M71*$^{+}$ ORN. 150 msec 300 µM niflumic acid was given at two different timings indicated by the junction current in red and blue on top. Blue dashed line marks the starting time of niflumic acid in blue trace. Arrow marks the time when blue and red traces started to overlap with each other. The time between the blue dashed line and the arrow is 65 msec, which is the time required for niflumic acid inhibition to reach a steady state. Currents after niflumic acid withdrawal were truncated for clarity. **B**, same trace as the control response in **A**, gray shaded area is 65 msec wide, indicating the window that niflumic acid inhibition effect cannot be measured accurately. Note that the shaded area encompasses the rising phase and the peak of the response. Timing of acetophenone is indicated above each panel by junction current measured with 90% Ringer. NFA: niflumic acid.

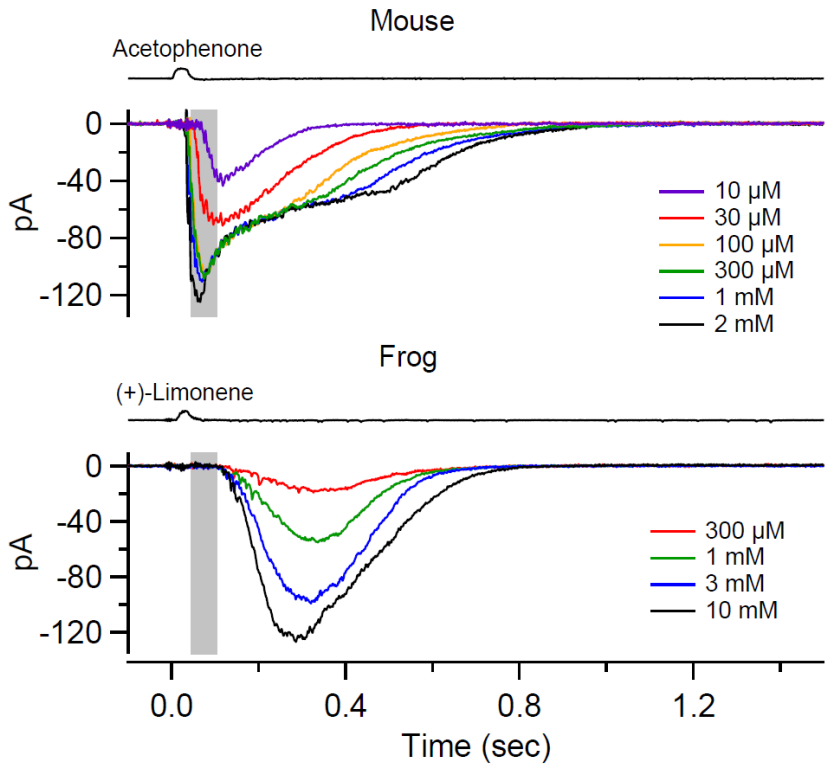

Fig. 4-4. Frog responses have delayed onset.

Response families from a *M71*$^{+}$ ORN (top) and a frog ORN (bottom) showed that the onset of mouse responses has almost no delay after odorant application but responses from frog ORN showed a delay of ~65 msec (between the end of the odorant pulse to the onset of the response). Shaded areas are 65 msec wide, corresponding to the dead time during which inhibition by niflumic acid is unreliable. The delayed onset of frog responses avoids this caveat. Timing of acetophenon or (+)-limonene application is indicated above each panel by junction current measured with 90% Ringer.

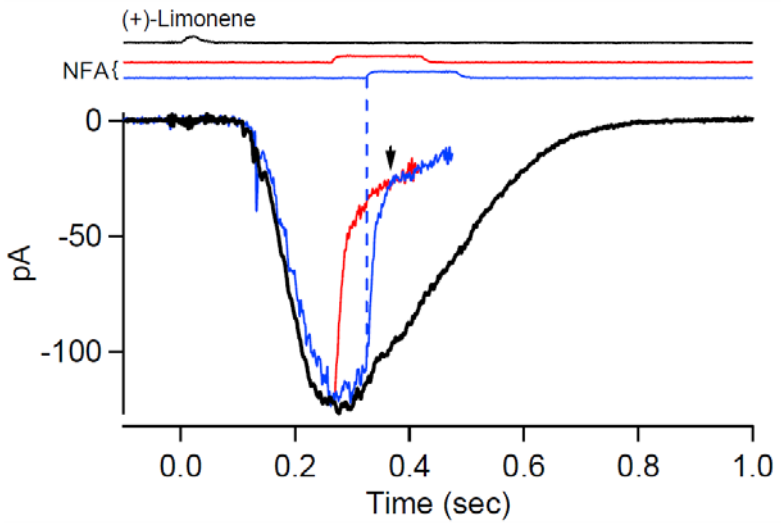

Fig. 4-5. Niflumic acid dead time in frog ORNs.

Odorant response from a frog ORN elicited by 10 mM (+)-limonene. Similar to Fig.4-3, blue dashed line marks the starting time of 300 μM niflumic acid to the blue trace. Arrow marks the time when red and blue traces first overlap. The time gap between the two is ~45 msec. Timing of (+)-limonene or niflumic acid is indicated above by junction current measured with 90% Ringer. NFA: niflumic acid.

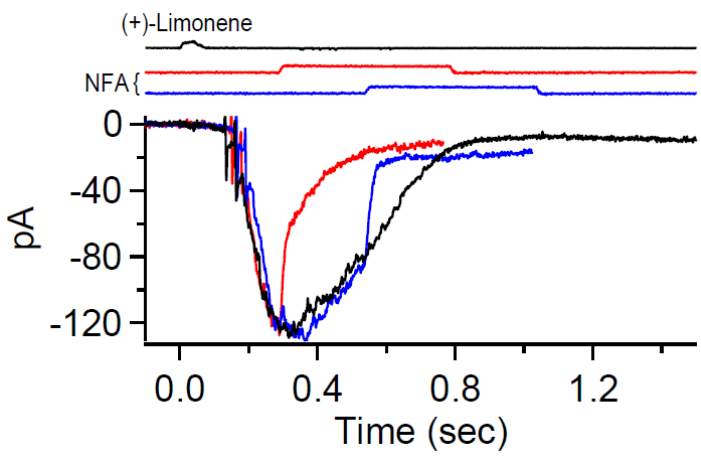

Fig. 4-6. Prolonged exposure to niflumic acid may have complications.

Niflumic acid (500 msec, 300 μM) was applied at 2 different time that are 250 msec apart (instead of 60 msec mentioned in Fig. 4-3 and Fig. 4-5), the red and blue traces no longer overlap with each other. Timing of (+)-limonene or niflumic acid is indicated above by junction current measured with 90% Ringer. NFA: niflumic acid.

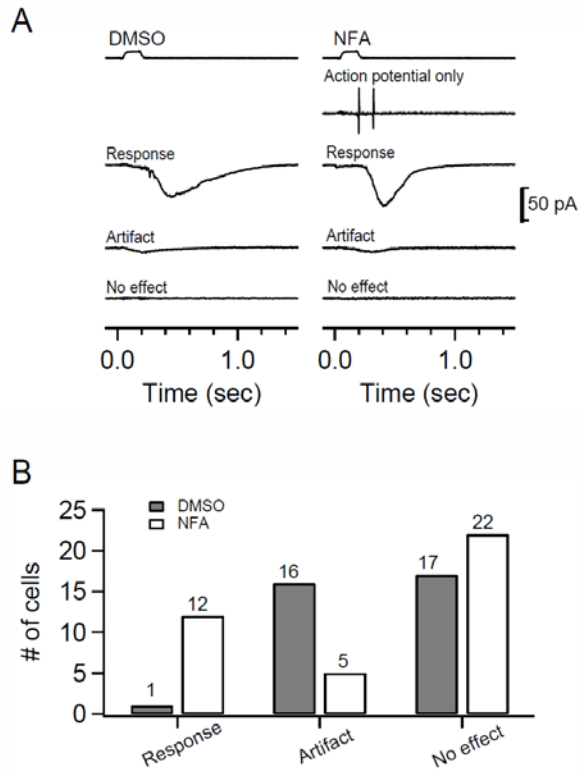

Fig. 4-7. Effect of DMSO and niflumic acid alone.

A. Frog ORNs were given 150 msec of 0.2% DMSO (left) or 300 μM niflumic acid (right). Three different consequences may be seen, a true odorant response, an artifact or no effect. The artifact usually presents as a small downward deflection of the trace of about 2-8 pA. The timing of occurrence is too fast to be an odorant response. Most of the time, cells responding to niflumic acid do not show apparent inward current, but a short train of action potentials (2-4 spikes). **B**. Quantitative data of **A**. Thirty-four cells were tested with DMSO and 39 cells were tested with niflumic acid. DMSO gave rise to transduction current in only 1 out 34 cells. Niflumic acid also triggered apparent transduction current in only 1 cell, but cells that only fire action potentials without apparent inward current upon niflumic acid exposure are also included in the 'response' group. Timing of DMSO or niflumic acid exposure is indicated above **A** by junction currents measured with 90% Ringer. NFA: niflumic acid.

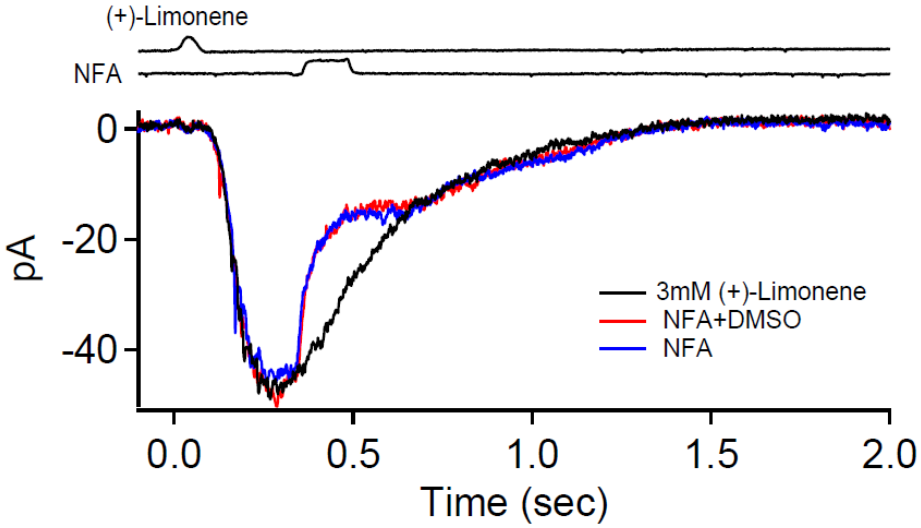

Fig. 4-8. Niflumic acid effect with and without DMSO.

Odorant responses were elicited by 30 msec of 3 mM (+)-limonene. 150 msec of 300 µM niflumic acid that was dissolved directly into Ringer or from stock solution prepared in DMSO (final concentration of DMSO is 0.2%) is applied during the odorant response. The inhibitory effect of niflumic acid in the absence or presence of 0.2% DMSO showed no difference. Timing of (+)-limonene or niflumic acid is indicated above by junction current measured with 90% Ringer. NFA: niflumic acid.

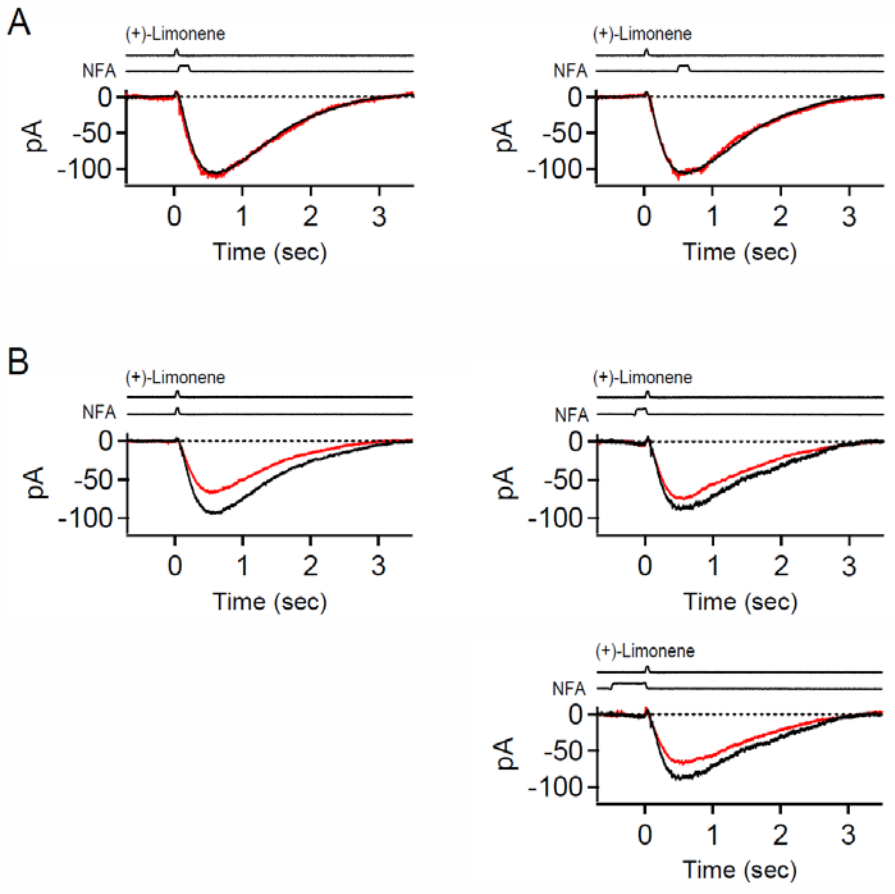

Fig. 4-9. Niflumic acid effect on CNG current in frog ORNs.

In a frog ORN, odorant response were elicited by 30 msec 3 mM (+)-limonene in 0-Ca^{2+} Ringer, therefore responses consist of CNG current only. **A**. 150 msec of 300 µM niflumic acid was given immediately after odorant pulse (left) or near the peak of response (right). Responses with niflumic acid exposure (red traces) showed no inhibition compared with odorant-only responses (black traces). **B**. 150 msec of 300 µM niflumic acid was given simultaneously with odorant pulse resulting in reduction of the response (left, red trace). 300 µM niflumic acid was given for 150 msec (upper) or 500 msec (lower) immediately before odorant pulse, which attenuated the odorant responses (red traces). Timing of (+)-limonene or niflumic acid application is indicated above each panel by junction current measured with 90% Ringer. NFA: niflumic acid.

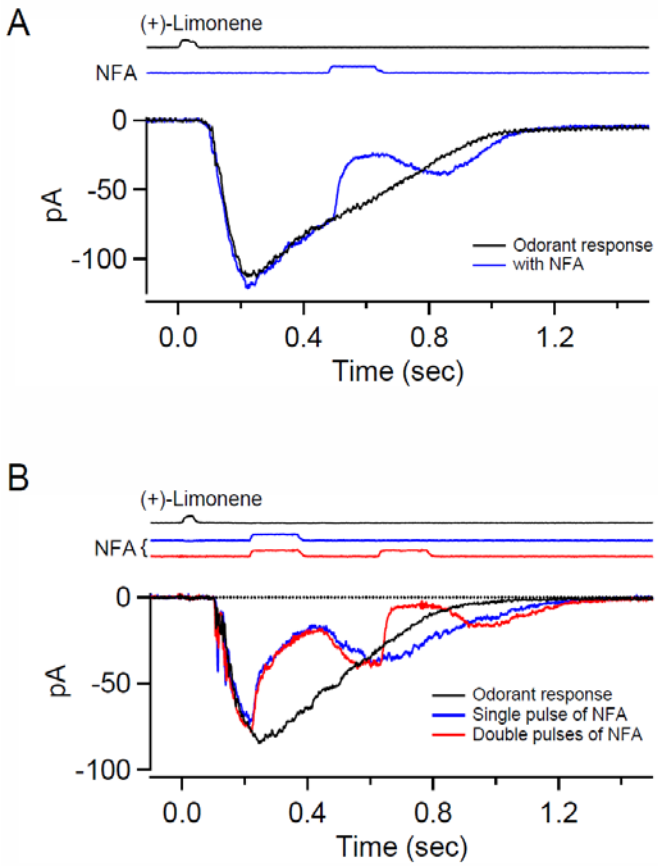

Fig. 4-10. Rebound current upon niflumic acid withdrawal.

A. Odorant response triggered by a 30 msec pulse of 3 mM (+)-limonene from a frog ORN (black trace). Application of 150 msec of niflumic acid results in reduction of the current followed by a current rebound upon niflumic acid withdrawal (blue trace). **B**. In a different cell, rebound is also observed when withdrawing niflumic acid (blue trace). A second pulse of 150 msec 300 µM niflumic acid given at the peak of the rebound, inhibited most of the rebound current, suggesting that the rebound consists of primarily Cl current. Timing of (+)-limonene or niflumic acid application is indicated above each panel by junction current measured with 90% Ringer. NFA: niflumic acid.

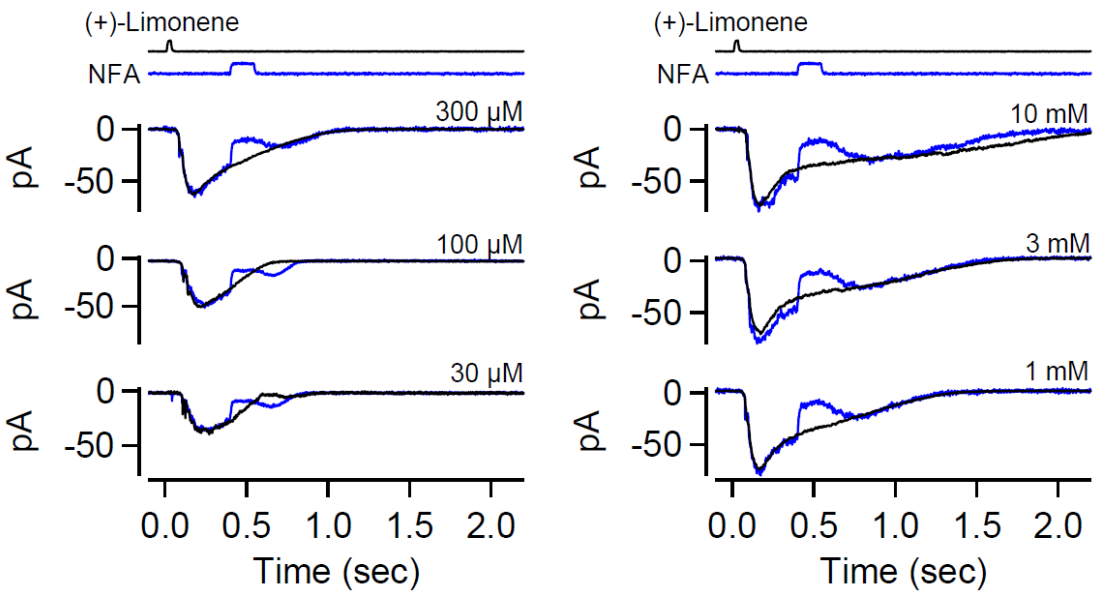

Fig. 4-11. Niflumic acid rebound reduces as response saturates.

Niflumic acid (150 msec, 300 µM) applied to odorant responses elicited by different concentrations of (+)-limonene. The magnitude of the rebound is negatively correlated with the strength of the odorant stimuli. In fact, in the responses from saturating stimuli (1mM, 3mM and 10 mM), no rebound was found. Timing of (+)-limonene or niflumic acid application is indicated above each panel by junction current measured with 90% Ringer. NFA: niflumic acid.

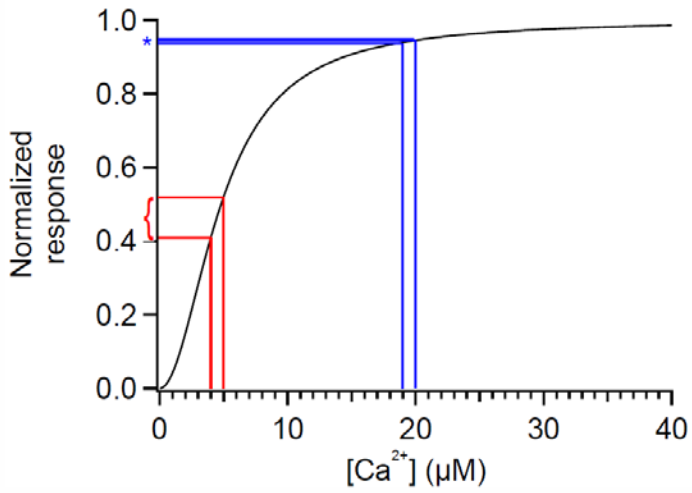

Fig. 4-12. Effect of intra-ciliary [Ca^{2+}] increase on Ano2 inversely correlates with degree of saturation.

Dose-response curve of Ano2 plotted with EC50: 4.8 μM and Hill coefficient: 2 (Kleene and Gesteland, 1991). It is clear that a small increment (for example 1 μM) in intra-ciliary [Ca^{2+}] gives large increase in Ano2 opening when Ano2 is not saturated (red bracket) compared with near saturation (blue *).

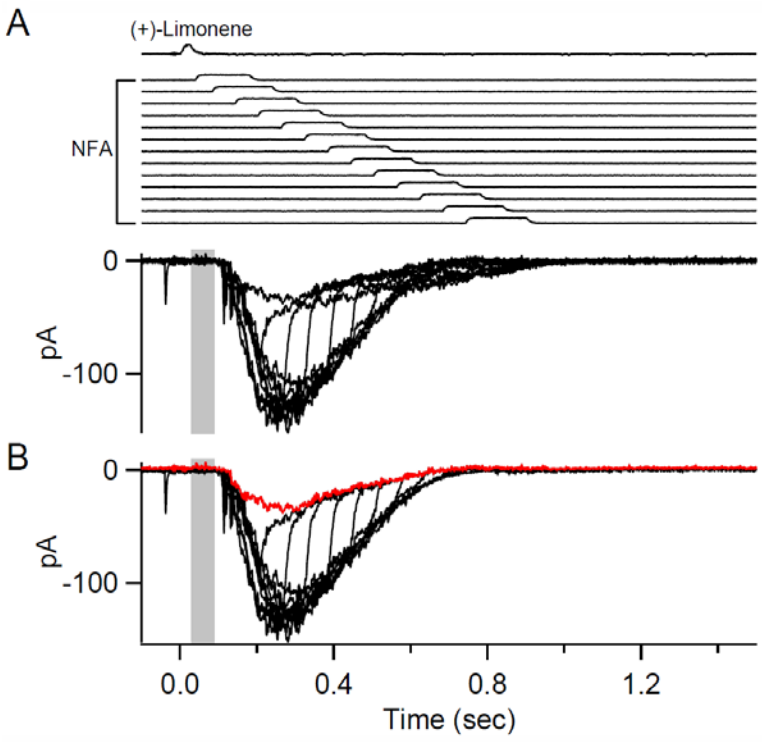

Fig. 4-13. Obtaining the envelope of residual current.

A. A series of 150 msec 300 µM niflumic acid each delayed by 60 msec was applied during the response elicited by 10 mM (+)-limonene. The residual currents during niflumic acid action overlap with one another, forming a continuous envelope. **B**. The envelope is highlighted in red to show the overall time course of the residual current. Currents after niflumic acid removal were truncated for clarity. The shaded area is the window when niflumic acid effect has not reached steady state. Note that the onset of transduction current is outside of the shaded area. Timing of (+)-limonene or niflumic acid application is indicated above by junction current measured with 90% Ringer. NFA: niflumic acid.

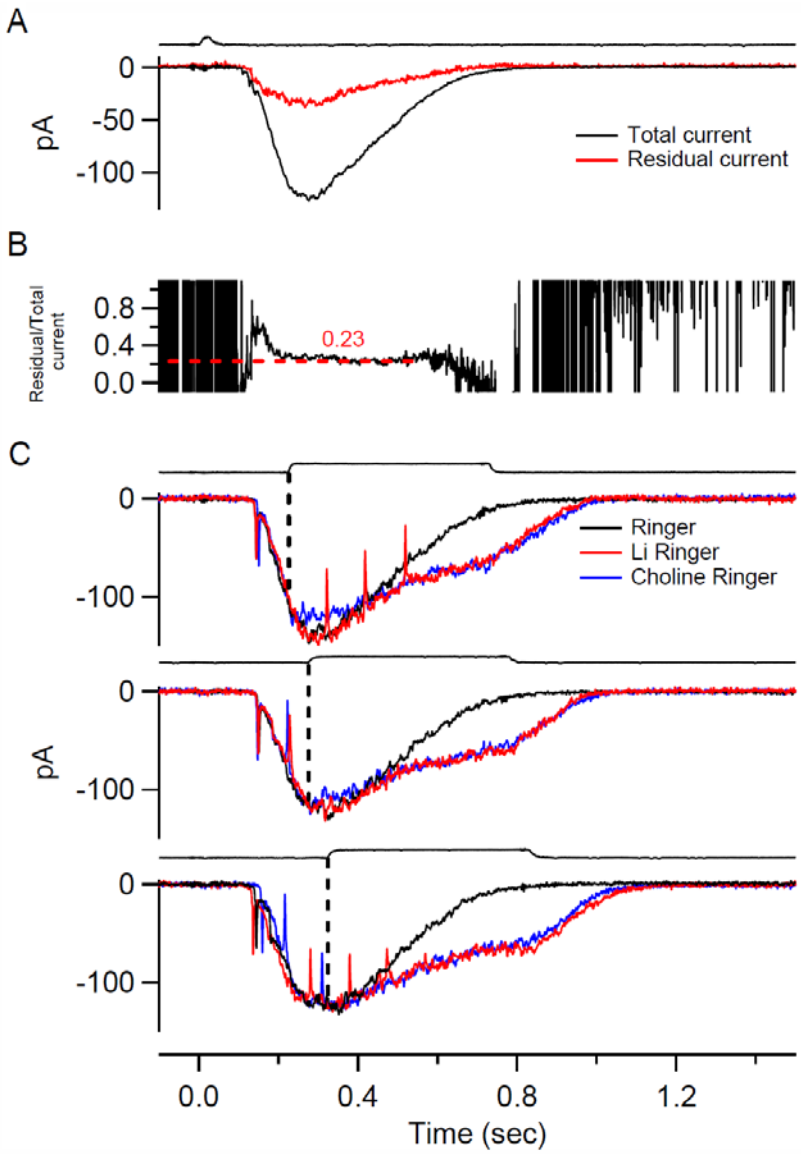

ig. 4-14. Tail of an odorant response has little if any CNG current.

Same cell as Fig. 4-13. **A**. Same response and envelope of residual current as Fig.4-13 were plotted again to give a reference to the time course. **B**. Dividing residual current by total current yielding the time course of the residual/total current. Note that the fraction became a constant (0.23) except for the beginning of the response. **C**. External solution was changed to either Li (red) or choline (blue) Ringer during the odorant response. **Upper and middle panel**, solution change was performed early in the response. After the solution change, current recorded in choline Ringer became smaller than the current

recorded in Li Ringer. Note that the relaxation phase of the response in Li Ringer is the same as that in choline Ringer, but it is significantly delayed compared with Na Ringer, which is due to NCKX4 not functioning in Li or choline Ringer. **Lower panel**, solution change performed at later time. Currents in Li and choline Ringer showed no obvious difference. Timings of (+)-limonene application and Li or choline solution change are indicated above the corresponding panel by junction current measured with 90% Ringer.

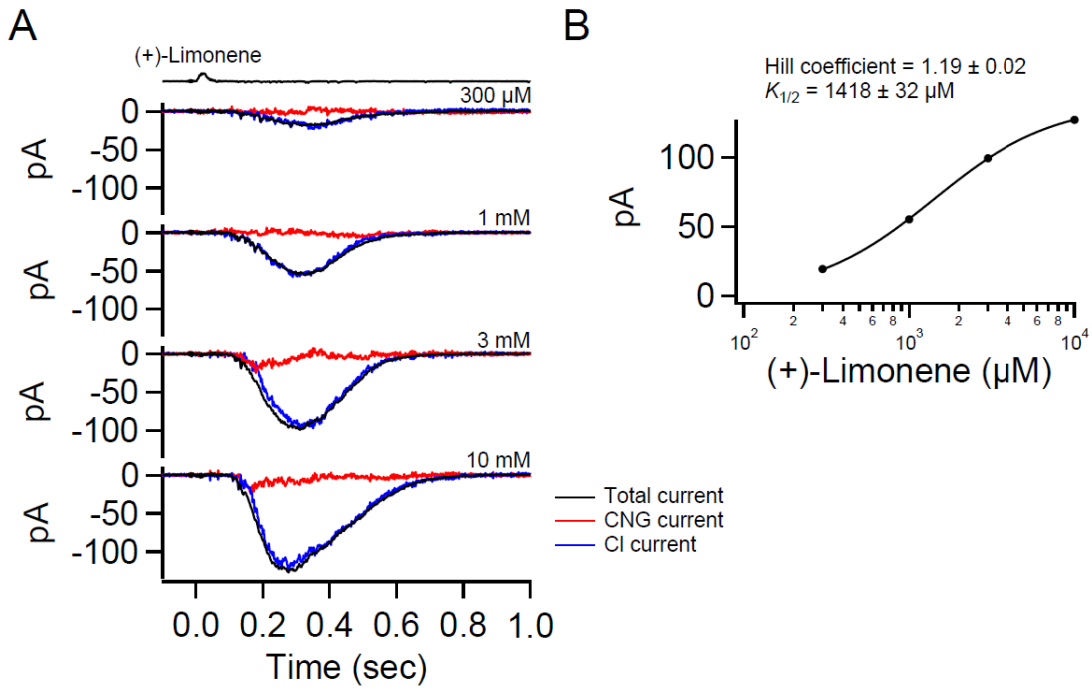

Fig. 4-15. Dissecting the transduction current into CNG and Cl currents.

Same cell as in Fig. 4-13 and Fig. 4-14. **A**, the response family dissected into CNG and Cl current. Note that Cl current makes up the majority if not entirely of the response. The peak of CNG current is much earlier than the Cl current. **B**. Stimulus-response curve of the total current showing that the cell has not reached saturation.

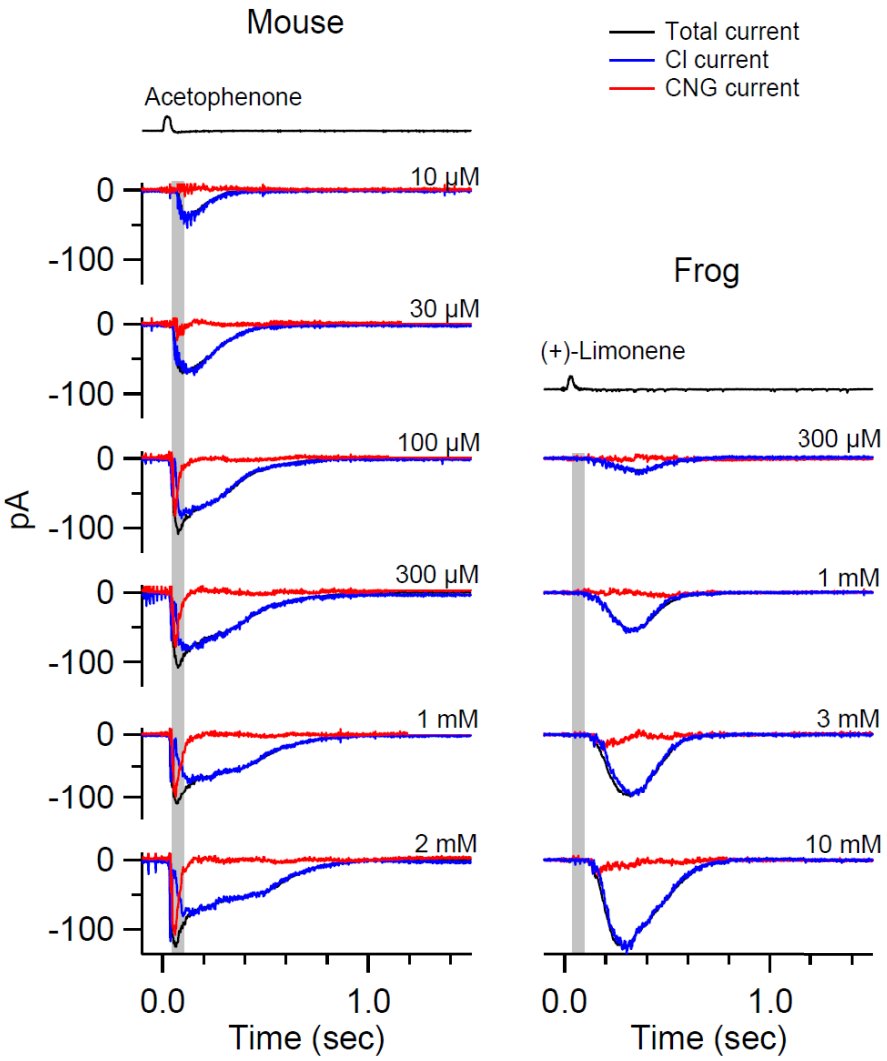

Fig. 4-16. Comparing the dissected response family of mouse and frog ORNs.

Same method can be applied to mouse ORNs as well. However, as previously discussed, the rising phase and peak of responses in mouse ORN (left) are within the niflumic acid dead time, making the dissection incomplete. Right, same frog ORN shown in Fig. 4-17, demonstrating that the dissection is complete, not affected by the dead time.

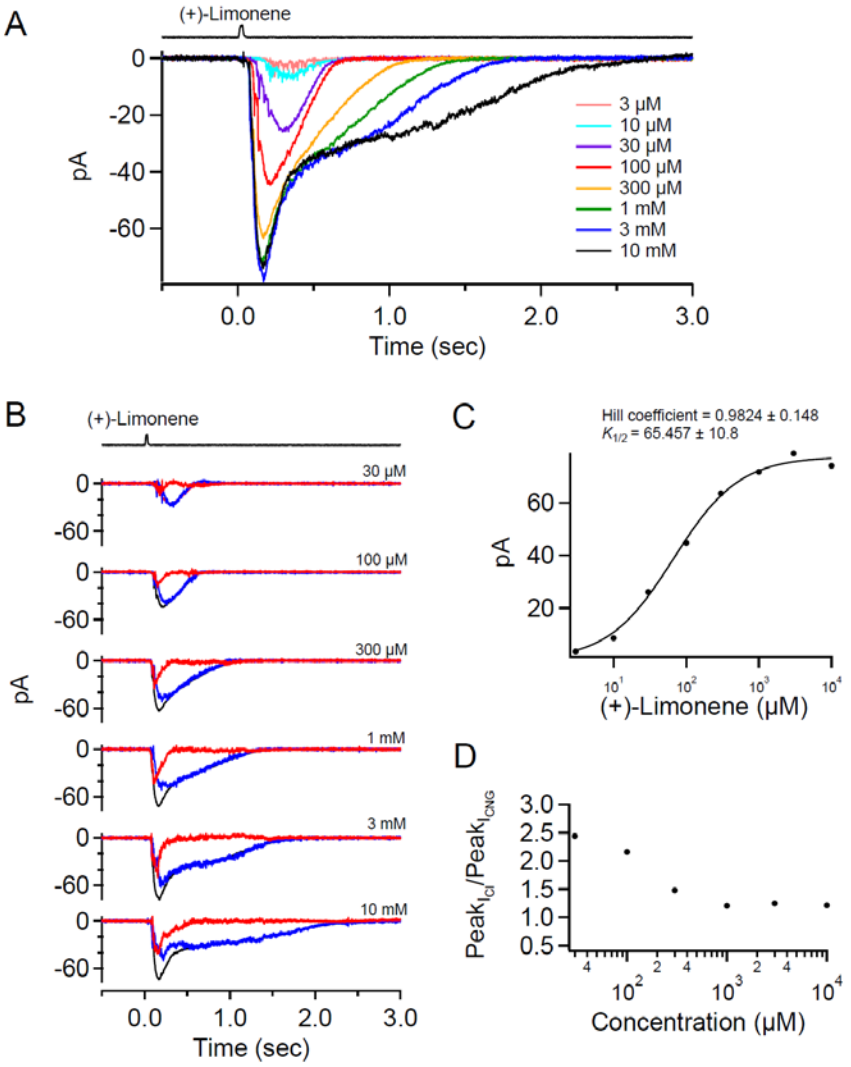

Fig. 4-17. Frog ORN with responses reaching saturation.

A. Response family of a frog ORN in which the responses reached saturation. **B**. Response family dissected into CNG and Cl currents. **C**. Stimulus-response curve of the total current. **D**. Ratio between Cl current and CNG current peak amplitudes. Note that the ratio became lower and reached a constant as stimulus strength is increased.

Chapter 5: Analysis of the kinetics of the response recovery

5.1 Introduction

It is known that the photoresponses in rod photoreceptors demonstrate an interesting phenomenon: for flash intensities ranging up to 2 log units, the final recovery phase of the saturated responses has invariant kinetics (Baylor et al., 1974; Pepperberg et al., 1992, 1994). In other words, the relaxation phase of a response elicited by flash intensity Φ looks the same as a response elicited by flash intensity Φ_0 after it is translated along the time axis. The amount of the shift can be given by $t_{shift} = \tau_c \ln(\Phi/ \Phi_0)$. This phenomenon was first observed and explain by Baylor et al. in 1974, followed by more elaborate mathematical analysis in the 1990s (Nikonov et al., 1998; Pepperberg et al., 1992, 1994), when it started to be called recovery translation invariance or RTI (Nikonov et al., 1998). The significance of this behavior is that it implies that one of the signal transduction steps dominates the recovery mechanism and this step decays exponentially with time constant τ_c . These analyses provided insights into the rate-limiting step of the deactivation processes of phototransduction.

In our results, we observed similar behavior in the olfactory transduction current, although slightly more complicated. We attempted to analyze the kinetics similar as was done for phototransduction.

5.2 Results

5.2.1 Ano2 inactivation or Cl^- depletion

The response families from one frog and two mouse ORNs are shown in Fig. 5-1. A phenomenon common to all three response families was observed, that is, as the response became saturated, the peak amplitude showed little increase, while the tails of the current continued to elongate, exhibiting two dominant phases of decay (marked 1 and 2, respectively).

If we just focus on the mouse ORN in Fig. 5-1, the currents during the first phase of decay overlapped with one another in the responses from the 3 highest concentrations. The second phase exhibits a faster relaxation than the first phase, with the response elicited by the weakest stimulus of the three deviating from first phase the earliest. From Chapter 4, we know that during these two phases only Cl current is present, so the kinetics entirely reflect the behavior of Cl current. During the first phase, all three traces overlapped with each other, suggesting either that the intra-ciliary Ca^{2+} concentration is the same at this time for all three traces, or Cl current is saturated. The fact that the second phase happened at different times with different stimulus intensities suggests that the intra-ciliary Ca^{2+} concentration cannot be the same for these responses. Therefore the Cl current is saturated in these three traces during the first phase. This suggests that for strong stimuli, the total Ca^{2+} influx is more than needed to saturate all the Cl channels. The first phase thus reflects the time when intra-ciliary Ca^{2+} still saturates the Cl channels. The second phase which the current deviated from the first phase indicates that Cl current no longer was saturated.

Interestingly, during the first phase when Cl current is saturated, the currents do not have flat plateaus but show gradual decline that have the same time course in all three traces. This decline may be attributed to Ano2 inactivation or depletion of intra-ciliary Cl^-. Both mechanisms have been suggested to take place in olfactory transduction (Vocke et al., 2013), although it is still not clear how important they are physiologically. Regardless of the detailed mechanism, it is clear the maximal available Cl current is limited by a declining process as a function of time, which is independent of stimulus intensity. We can fit the decay by a single exponential decay, $I_{Cl.decay}$ (Fig. 5-2, dashed line), which can be described as the following equation:

$$I_{Cl.decay} = I_{Cl.Max} e^{-t/\tau_{Cl}}$$

where $I_{Cl.decay}$ is the time course of the decay of the saturated Cl current, $I_{Cl.Max}$ is where the fit intersects with the y-axis at $t = 0$[1] , and τ_{Cl} is the time constant.

5.2.2 Olfactory transduction response obeys recovery translation invariance

To simplify our analysis of the recovery phase, we normalized the response family to the exponential fit (Fig. 5-3A). The logic is to examine the recovery kinetics as if Ano2 does not inactivate and/or there is no Cl^- depletion. This action is legitimate because the Cl

[1] $I_{Cl.Max}$ is not the saturated Cl current. Ideally, we should describe the decay of the saturated Cl current by $I_{Cl.decay} = I_{Cl.sat} e^{-(t-t_0)/\tau_{Cl}}$, where $I_{Cl.decay}$ is the time course of the decay of the saturated Cl current, $I_{Cl.sat}$ is the saturated Cl current if no decay happens , τ_{Cl} is the time constant, and t_0 is the time when the decay of Cl current begins. However, one can rewrite the equation as the following, $I_{Cl.decay} = I_{Cl.sat} e^{-(t-t_0)/\tau_{Cl}} = I_{Cl.sat} e^{t_0/\tau_{Cl}} e^{-t/\tau_{Cl}} = I_{Cl.Max} e^{-t/\tau_{Cl}}$, where $I_{Cl.sat} e^{t_0/\tau_{Cl}} = I_{Cl.Max}$. Because $I_{Cl.sat}$ and t_0 are both free parameters, without correct boundary conditions, we cannot determine the correct combination of $I_{Cl.sat}$ and t_0 through fitting the curves. Hence we just use $I_{Cl.Max}$ and τ_{Cl} for fitting the decay.

current decay is a process that is independent of the stimulus intensity, unlike the process of RTI.

After normalization, it is obvious that the recovery phases of the saturated responses follow the same time course, at least over a range of odorant concentrations. In fact, one can shift the response family so the tails largely superimpose with each other (Fig. 5-3B), similar to what was found in the rod and cone photoreceptors (Adelson, 1982a, 1982b; Baylor et al., 1974; Nikonov et al., 1998; Pepperberg et al., 1992).

Pepperberg plot, the method used in phototransduction field (Pepperberg et al., 1992, 1994) to analyze the recovery phase of the response family, was adopted for our own analysis after it was normalized by $I_{Cl.decay}$. To determine the relationship between the time shift and the intensity of stimulation, we defined several critical levels (0.2, 0.3 and 0.4 in this case) and mark the time when the critical levels intersects with recovery phases of the responses. The timing of the intersections and the stimulus intensity have a linear relation on a semi-log plot (Fig. 5-4B). The relation between the timing of intersection can thus be described by the following equation

$$t = \tau_c \ln(\Phi) + C \qquad (5.1)$$

Where Φ is the odorant concentration, t is the timing of the intersection, C is a constant, and τ_c is the slope derived from Fig. 5-4B (τ_c, c stands for critical, because of **c**ritical level). For 3 different critical levels chosen (0.2, 0.3 and 0.4 of the normalized response), τ_c is around 0.1 sec for this cell. From analysis in phototransduction, τ_c, which dictates the translational increment in RTI, is the longest time constant of the signal transduction

steps, or the rate-limiting step for transduction shut off (Nikonov et al., 1998). This suggests that the rate limiting step for olfactory transduction termination likely decays with time constant on the order of 0.1 sec, although we do not know which step it is. It should be pointed out that directly fitting the final decaying phase of the currents give time constants that are different from τ_c (Fig. 5-4C). This will be explained in the next section.

5.3 Discussion: another implication of RTI from mathematical analysis

We adopted the mathematical framework of Nikonov, Enheta and Pugh, and conducted the following analysis.

From equation (5.1), the timings, t_0 and t, where a critical level intersects with responses given by two different saturating stimulus concentrations, Φ_0 and Φ can be written as the following equations

$$t_0 = \tau_c \ln(\Phi_0) + C$$
$$t = \tau_c \ln(\Phi) + C$$

The time shift, t_{shift}, between the two responses will be

$$t_{shift} = t - t_0$$
$$= \tau_c \ln(\Phi) + C - \tau_c \ln(\Phi_0) - C$$

This gives

$$t_{shift} = \tau_c \ln(\frac{\Phi}{\Phi_0}) \qquad (5.2)$$

If we define the recovery time course of a saturated response elicited by odorant concentration Φ_0 being $I_{Cl.0}[t]$, we can describe the recovery phase of any other saturated response in the family with stimulus Φ by the following equation

$$I_{Cl.\Phi.0}[t] = I_{Cl}\ [t - \tau_c \ln(\frac{\Phi}{\Phi_0})] \tag{5.3}$$

This means that at the recovery phase of the response elicited by intensity Φ is equivalent to shifting the response elicited by intensity Φ_0 to the right by $t_{shift} = \tau_c \ln(\Phi/\Phi_0)$. In other words, this is the equation that defines RTI.

We can rewrite equation (5.3) as the following

$$\begin{aligned} I_{Cl.\Phi.0}[t] &= I_{Cl}\ [t - \tau_c \ln(\frac{\Phi}{\Phi_0})] \\ &= I_{Cl.0}[-\tau_c(\frac{-t}{\tau_c} + \ln(\frac{\Phi}{\Phi_0}))] \\ &= I_{Cl.0}[-\tau_c(\ln(e^{-t/\tau_c}) + \ln(\frac{\Phi}{\Phi_0})] \\ &= I_{Cl.0}[-\tau_c \ln(\frac{\Phi}{\Phi_0} e^{-t/\tau_c})] \end{aligned}$$

Let $I_{Cl.0}[t] = H[\ \ _0 e^{-t/\tau_c}]$, then the above equation can be written as

$$I_{Cl.\Phi.0}[t] \Phi\ I_{Cl}\ [t - \tau_c \ln(\frac{\Phi}{\Phi_0})] = H[\ \ e^{-t/\tau_c}] \tag{5.4}$$

This means that if a response family follows RTI, then the recovery phase can be described by a function with independent variable $\Phi e^{-t/\tau_c}$. In our case, it implies that an intermediate in the signal transduction cascade is proportional to the stimulus intensity (at least for the range that RTI holds) and it decays exponentially with time constant τ_c.

In fact, if a transduction intermediate has the above properties, then the resultant time course of the transduction current will always follow RTI.

$$
\begin{aligned}
H[\Phi e^{-t/\tau_c}] &= H[\ {}_0 \frac{\Phi}{\Phi_0} e^{-t\ {}_c}\ ] \\
&= H[\Phi_0 e^{\ln(\frac{\Phi}{\Phi_0}) e^{-t\ {}_c}}\ ] \\
&= H[\Phi_0 e^{-[\tau \ln(_c\ \tau)] \frac{\Phi}{\Phi_0}\ {}_c}\ ] \\
&= \mathrm{I}_{Cl.0}[t - \tau_c \ln(\frac{\Phi}{\Phi_0})]
\end{aligned}
$$

It should be pointed out that the Cl current recovery phase does not necessarily relax with the time constant τ_c, rather, the relaxation is determined by the *H* function. In phototransduction, the *H* function has properties that preserve τ_c as the time constant for final decay of the transduction current, however, the same may not apply to olfactory transduction, as seen in Fig 5-4C.

Consider the known olfactory transduction cascade in Fig. 5-5. An intermediate that is proportional to the odorant concentration has to be O·R*, G_{olf}*, or ACIII*, because components downstream give rise to non-linear amplification. In fact, because an activated O·R* complex can activate at most one G_{olf} molecule (Bhandawat et al., 2005) and the relationship between G_{olf} and ACIII is also one to one, if the amount of any one of the three is proportional to Φ, then the other two will be proportional to Φ as well. Simply, the amount of O·R* complex has to be proportional to Φ.

It is then interesting to check whether the amount of O·R* complex is indeed proportional to Φ. Consider a pulse of odorant concentration [O] was given for duration

T_P. Assume that solution change completes instantaneously and the concentration [O] remains a constant during the pulse because of the continuous laminar flow (see method). Then odorant binding and odorant-receptor complex activation reactions can be written as the following

$$O+R \underset{k_{off}}{\overset{k_{on}}{\rightleftarrows}} O \cdot R \underset{\beta}{\overset{\alpha}{\rightleftarrows}} O \cdot R^*$$

where O stands for odorant, R for receptor, O·R is the odorant-receptor complex in its inactive state, O·R* is the odorant-receptor complex in its active state, k_{on} and k_{off} are the rate constants for the binding and unbinding reactions, and α and β are the rates for forward and reverse reactions between inactive and active states of the odorant-receptor complex. If the reaction quickly reaches equilibrium at the end of the odorant pulse, then the amount of O·R* will be in the form of Michaelis Equation

$$O \cdot R^* = \frac{O \cdot R^*_{max}[O]}{[O] + K_{1/2}}$$

$$O \cdot R^*_{max} = \frac{\alpha R_T}{(\alpha + \beta)} \text{ and } K_{1/2} = \frac{\beta k_{off}}{(\alpha + \beta) k_{on}}$$

where R_T is the total number of odorant receptor molecule and $K_{1/2}$ is the half-saturation constant for odorant-receptor binding (not to be confused with the half-saturation constant for transduction current) and $O \cdot R^*_{max}$ is the maximal possible number of O·R*.

Only when $[O] << K_{1/2}$ will the amount of O·R* be approximately proportional to [O]. The $K_{1/2}$ for most ORs is unknown, but a fish OR, 5.24, that detects amino acids was found to have nanomolar range of $K_{1/2}$ (Kuang et al., 2003). However, RTI occurs when

odorant stimulus is at supra-saturating concentration, (millimolar) range, which is unlikely to be much lower than $K_{1/2}$.

An alternative scenario can also result in O·R* being approximately proportional to [O]. The Michaelis Equation only describes the steady state, when ligand-receptor binding reaches equilibrium. However, in our experiments, we applied very brief pulses of odorant such that the odorant-receptor binding may not reach equilibrium. In this context, for stimulation duration, $T_{p,}$ that is much shorter than the time constants of the binding/activation process odorant-receptor complex, one can demonstrate that at the end of the stimulation pulse, the amount of O·R* is much smaller than total number of receptor, and O·R* can be expressed as the following (please see appendix for detail analysis)

$$\mathrm{O}\cdot\mathrm{R}^* \approx \frac{\alpha k_{on} \mathrm{R}_\mathrm{T} T_\mathrm{p}^{\,2}[\mathrm{O}]}{2}$$

which is indeed proportional to [O]. This holds true even if a very high concentration of odorant is applied, as long as T_p is much short than the time constant of the binding/activation process of odorant-receptor complex

We still do not have enough evidence to determine which scenario is happening in our system. For both cases, it is clear that with a brief pulse of odorant, the amount of activated odorant-receptor complex has to be very low even when the cell is stimulated with a very high concentration of odorant.

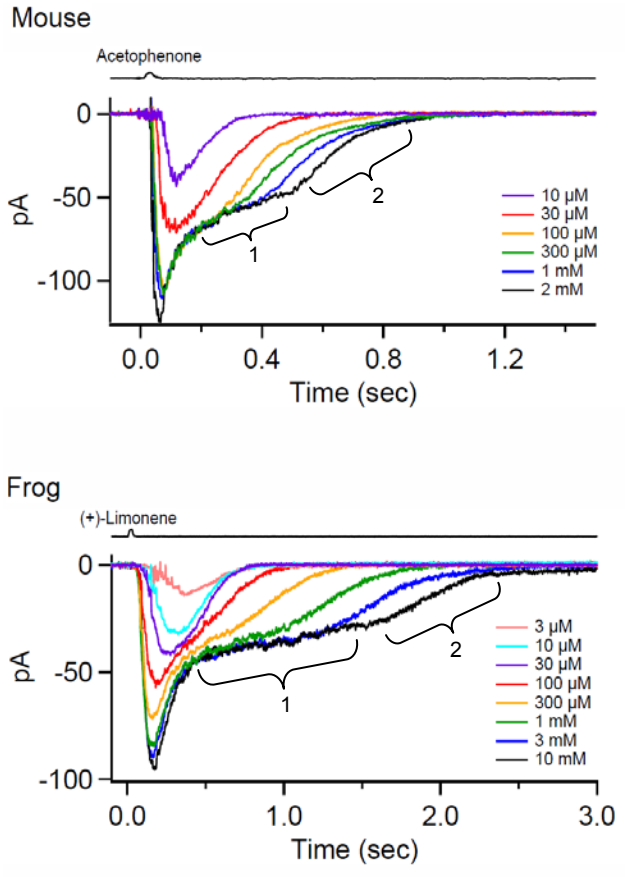

Fig. 5-1. Saturated response families of mouse and frog ORNs.

Response families from one mouse and one frog ORN are shown. The response families demonstrate a gradually prolonged tail with two phases of decay (marked with 1 and 2) as the stimulation gets stronger.

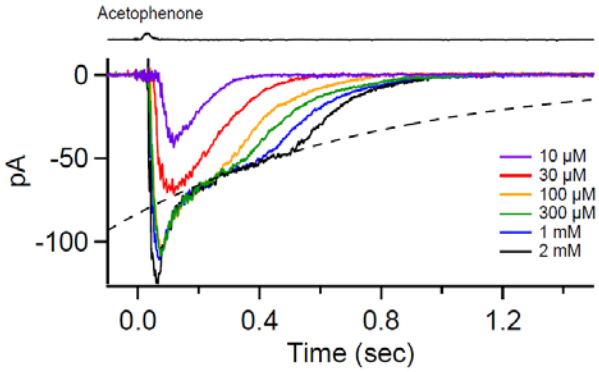

Fig. 5-2. The first phase of decay can be fit with a single exponential.

The same mouse ORN showed in Fig.5-1. Dashed line is fit of a single exponential.

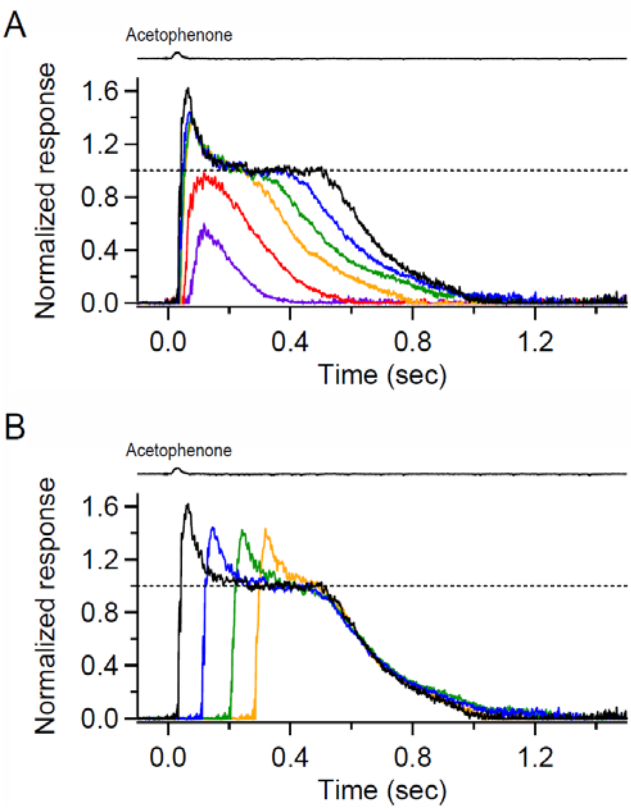

Fig. 5-3. The ORN response family has similar relaxation kinetics after correcting for Cl current desensitization/Cl depletion. A. Response family shown in Fig.5-2 was normalized to the exponential fit. Note that the first phase of decay is now a flat plateau. **B**. Translating the saturated responses along the time axis demonstrates that they recover with a similar time course.

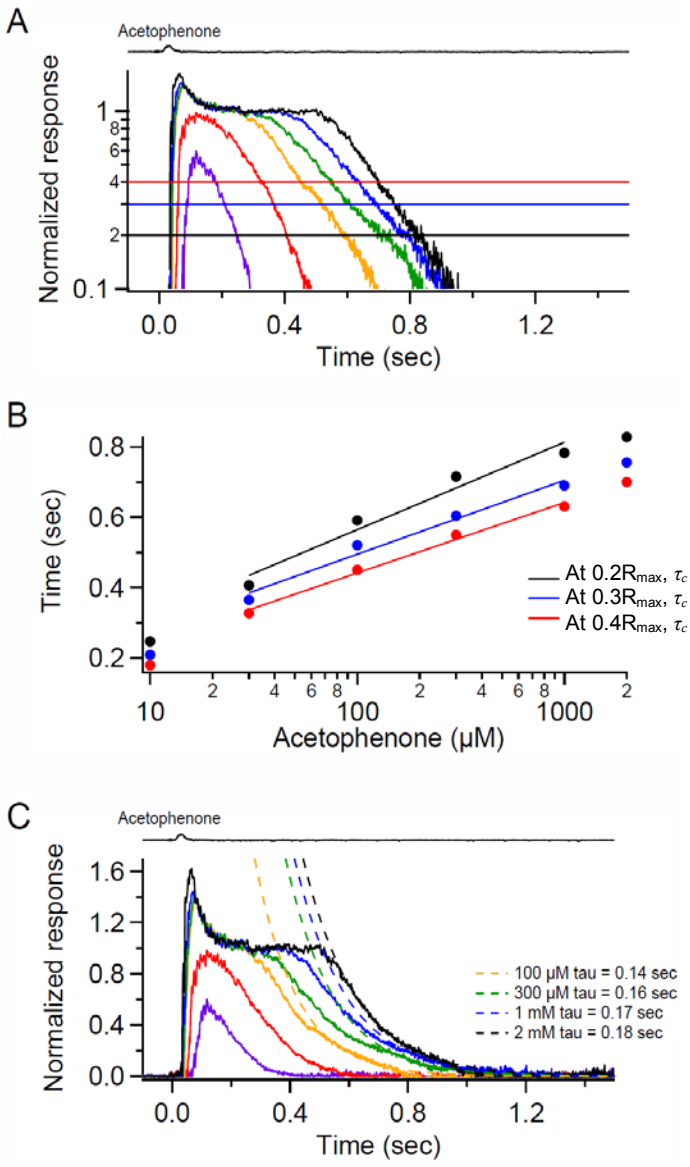

Fig. 5-4. The saturated responses obey recovery translation invariance.

A. Critical levels at the 0.2, 0.3 and 0.4 were selected (black, blue and red horizontal lines). Note that y-axis is changed to logarithmic to emphasize the range of the critical levels chosen. **B**. The timing points at which the recovery phases intersect with different critical levels were plotted against stimulus concentration in a semi-log plot. The relation can be fit with a straight line, with the slope τ_c being 0.11, 0.09 and 0.09 sec respectively. R_{max}: maximal response. **C**. Directly fitting the recovery phase with exponentials to obtain the decay time constant.

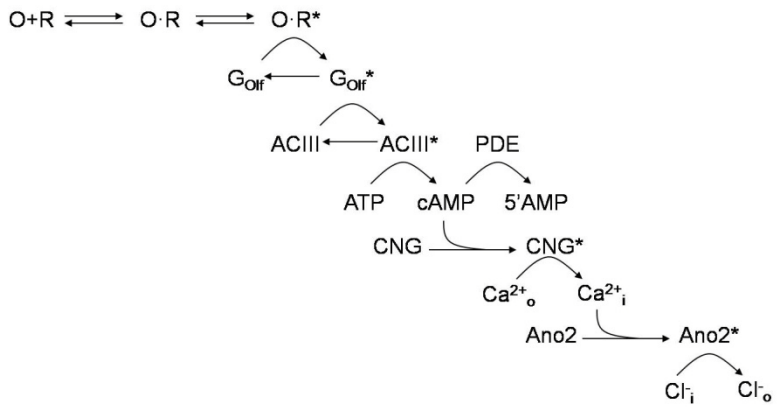

Fig. 5-5. Scheme of the olfactory transduction cascade.

O: odorant. O·R: odorant-receptor complex. Molecules marked with * sign are in their activated form.

5.4 Appendix:

The amount of odorant-receptor complex in the active state as a function of time

We started by considering an odorant stimulation of concentration [O] that was given for duration T_P. Assume that solution change completed instantaneously and the concentration remained a constant during stimulation because of the continuous laminar flow (see method). Then odorant binding and odorant-receptor complex activation reactions can be written as the following

$$\mathrm{O+R} \underset{k_{off}}{\overset{k_{on}}{\rightleftarrows}} \mathrm{O\cdot R} \underset{\beta}{\overset{\alpha}{\rightleftarrows}} \mathrm{O\cdot R^*}$$

where O stands for odorant, R for receptor, O·R is the odorant-receptor complex in its inactive state, O·R* is the odorant-receptor complex in its active state, k_{on} and k_{off} are the rate constants for the binding and unbinding reactions, and α and β are the rates for forward and reverse reactions between inactive and active states of the odorant-receptor complex. The amount of O·R* change through time can be described by the following =equations

$$\frac{d(\mathrm{O\cdot R^*})}{dt} = \alpha(\mathrm{O\cdot R}) - \beta(\mathrm{O\cdot R^*}) \tag{i.1}$$

$$\frac{d(\mathrm{O\cdot R})}{dt} = k_{on}[\mathrm{O}]\mathrm{R} - k_{off}(\mathrm{O\cdot R}) + \beta(\mathrm{O\cdot R^*}) - \alpha(\mathrm{O\cdot R}) \tag{i.2}$$

with the following boundary conditions

when $t = 0$, $\mathrm{O\cdot R^*} = 0$, $\mathrm{O\cdot R} = 0$

when $t = \infty$, $\frac{d(\mathrm{O\cdot R^*})}{dt} = 0$, $\frac{d(\mathrm{O\cdot R})}{dt} = 0$

Total number of receptor, R_T, has the following relation

$$\mathrm{R_T} = \mathrm{O\cdot R^*} + \mathrm{O\cdot R} + \mathrm{R} \tag{i.3}$$

Combining equations (i.1) and (i.3) gives

$$(\mathrm{O}\cdot\mathrm{R}) = \frac{1}{\alpha}[\frac{d(\mathrm{O}\cdot\mathrm{R}^*)}{dt} + \beta(\mathrm{O}\cdot\mathrm{R}^*)] \qquad \text{(i.4)}$$
$$\mathrm{R} = \mathrm{R}_\mathrm{T} - \mathrm{O}\cdot\mathrm{R}^* - \mathrm{O}\cdot\mathrm{R}$$

Substituting (i.4) into (i.2) will give

$$\frac{d^2(\mathrm{O}\cdot\mathrm{R}^*)}{dt^2} + (k_{on}[\mathrm{O}] + k_{off} + \alpha + \beta)\frac{d(\mathrm{O}\cdot\mathrm{R}^*)}{dt} \qquad \text{(i.5)}$$
$$+[k_{on}(\alpha+\beta)[\mathrm{O}] + \beta k_{off}](\mathrm{O}\cdot\mathrm{R}^*) - \alpha k_{on}[\mathrm{O}]\mathrm{R}_\mathrm{T} = 0$$

This is actually a second order differential equation in the form of

$$\frac{d^2y}{dt^2} + B\frac{dy}{dt} + Cy + D = 0$$

where $B = k_{on}[\mathrm{O}] + k_{off} + \alpha + \beta$, $C = k_{on}(\alpha+\beta)[\mathrm{O}] + \beta k_{off}$, $\mathrm{D} = -\alpha\, k_{on}[\mathrm{O}]\mathrm{R}_\mathrm{T}$

The solution of this second order differential equation depends on $B^2 - 4C$. Let $[\mathrm{O}]k_{on} = k$, we have

$$\begin{aligned}
B^2 - 4C &= (k + k_{off} + \alpha + \beta)^2 - 4[\alpha k + \beta(k + k_{off})] \\
&= [(k + k_{off}) + (\alpha + \beta)]^2 - 4[\alpha k + \beta(k + k_{off})] \\
&= (k + k_{off})^2 + (\alpha + \beta)^2 + 2(k + k_{off})(\alpha + \beta) - (4\alpha k + 4\beta k + 4\beta k_{off}) \\
&= (k + k_{off})^2 + (\alpha + \beta)^2 - 2\alpha k - 2\alpha k_{off} - 2\beta k - 2\beta k_{off} + 4\alpha k_{off} \\
&= (k + k_{off})^2 + (\alpha + \beta)^2 - 2(k + k_{off})(\alpha + \beta) + 4\alpha k_{off} \\
&= [(k + k_{off}) - (\alpha + \beta)]^2 + 4\alpha k_{off} \\
&> 0
\end{aligned}$$

So the solution to this differential equation is the following

$$\mathrm{O}\cdot\mathrm{R}^* = \mathrm{O}\cdot\mathrm{R}^*_e\left(1 - \frac{a_2}{a_2 - a_1}e^{-a_1 t} - \frac{a_1}{a_1 - a_2}e^{-a_2 t}\right) \qquad \text{(i.6)}$$

where $a_1 = \dfrac{B + \sqrt{B^2 - 4C}}{2}$, $a_2 = \dfrac{B - \sqrt{B^2 - 4C}}{2}$, and

$O \cdot R^*_e = -\frac{D}{C} = \frac{\alpha k_{on}[O]R_T}{k_{on}(\alpha+\beta)[O]+\beta k_{off}}$, is the amount of O·R* at equilibrium.

Also note that $a_1 = 1/\tau_1$, $a_2 = 1/\tau_2$ are the reciprocal of the time constant for each exponential term.

The amount of O·R* at the end of T_p is

$$O \cdot R^*_{T_p} = \frac{\alpha k_{on}[O]R_T}{k_{on}(\alpha+\beta)[O]+\beta k_{off}}\left(1-\frac{a_2}{a_2-a_1}e^{-a_1T_p}-\frac{a_1}{a_1-a_2}e^{-a_2T_p}\right)$$
$$= \frac{\alpha[O]R_T}{(\alpha+\beta)([O]+\frac{\beta k_{off}}{(\alpha+\beta)k_{on}})}\left(1-\frac{a_2}{a_2-a_1}e^{-a_1T_p}-\frac{a_1}{a_1-a_2}e^{-a_2T_p}\right)$$

This can be proportional to [O] if

$$[O] << \frac{\beta k_{off}}{(\alpha+\beta)k_{on}} \qquad \text{(i.7)}$$

But from RTI, we know that even at millimolar range, $O \cdot R^*_{T_p} \propto [O]$ holds, making (i.7) unlikely. This brings the other possibility, which is having $T_p << 1/a_1$, $1/a_2$, or $a_1 T_p$, $a_2 T_p << 1$.

If $a_1 T_p$, $a_2 T_p << 1$, we can expand the exponentials as the first 3 terms of their power series

$$
\begin{aligned}
\mathrm{O}\cdot\mathrm{R}^*_{T_p} &\approx \mathrm{O}\cdot\mathrm{R}^*_e\left(1-\frac{a_2}{a_2-a_1}(1-a_1T_p+\frac{a_1{}^2T_p{}^2}{2})-\frac{a_1}{a_1-a_2}(1-a_2T_p+\frac{a_2{}^2T_p{}^2}{2})\right)\\
&=\frac{a_1a_2}{2}T_p{}^2\mathrm{O}\cdot\mathrm{R}^*_e\\
&=\frac{C}{2}T_p{}^2(-\frac{D}{C})\\
&=\frac{\alpha k_{on}[\mathrm{O}]\mathrm{R}_\mathrm{T}T_p{}^2}{2}\\
&=\frac{\alpha k_{on}\mathrm{R}_\mathrm{T}T_p{}^2}{2}[\mathrm{O}]
\end{aligned}
$$

This shows that if $a_1 T_p$, $a_2 T_p \ll 1$, the amount of O·R* is proportional to the stimulation concentration [O].

Chapter 6 Discussion

Niflumic acid has been widely used as a generic inhibitor of Ca^{2+}-activated Cl channels (Boccaccio and Menini, 2007; Kleene, 1993; Lowe and Gold, 1993; Sagheddu et al., 2010b). However, its specificity and efficacy has been under debate (Billig et al., 2011). Our detailed characterization of niflumic acid demonstrated that it does not block CNG current itself, but likely interferes with the interaction between odorant and odorant receptor or any signal transduction cascades upstream of CNG channel opening. Therefore, timing of niflumic acid application is of crucial importance to avoid confounding results. Our finding hopefully puts the final note to the doubt and points out the possible complications when niflumic acid is used in biological experiments in the future.

We developed a method to dissect CNG and Cl current in an odorant response, which gave a more accurate view of the amplification process from CNG signal to the final transduction current. One of our goals was to examine the CNG current kinetics, especially in the weak responses. Unfortunately, our method has intrinsic limitations, which, by dividing the original recorded signal with a factor less than 1 (1-fixed fraction of residual/total current), we are amplifying the noise. For large responses, the effect may be negligible. However, for weak responses, increased noise rendered detail analysis of the CNG current kinetics, particularly the relaxation phase, impossible. Additionally, the method cannot be applied to mouse ORNs due to the faster onset of odorant response, which is shorter than the time required for the inhibitory effect of niflumic acid to reach steady state. Despite these shortcomings, we were able to obtain information about the

overall duration of CNG current, which is very short compared with Cl current. We also demonstrated that the time-to-peak of an odorant response is first dictated by Cl current in weak stimulations, and dominated by CNG current as the stimulus strength increases. Importantly, in weak responses, the transduction current is almost entirely composed of Cl current. This showed that CNG current that is near or below our detection limit (~1 pA) is enough to trigger an apparent Cl current. The system is indeed designed to have a very sensitive amplification mechanism. It remains a question whether such amplification by Cl current really is physiologically relevant to land-based animals. On the other hand, water-based animals, such as frogs, undoubtedly benefit tremendously from this design.

Several directions can be pursued following current project. First of all, we plan to find out whether the sensitivity of *Ano2*$^{-/-}$ animals is indeed unchanged. From our preliminary results, at least at single-cell level, *Ano2*$^{-/-}$ ORNs required similar amount of current to depolarize the cell to change the firing rate beyond 2 standard deviations of the basal firing rate. This implies that more receptors should be activated to reach the threshold because the current generated per activated receptor in *Ano2*$^{-/-}$ is expected to be smaller than that in wild-type. Because *Ano2*$^{-/-}$ mice showed no detectable deficits in behavioral experiments, it will be interesting to learn at which level the olfactory system compensated for the change at the single-cell level. We are now collaborating with others to measure the threshold at the next level, the olfactory bulb, with Ca^{2+} imaging, so we can gain a better understanding of the sensitivity of *Ano2*$^{-/-}$ animals.

Second, we are setting up breeding between Ano2$^{-/-}$ and mice with PDE1C knocked-out, PDE4A knocked-out, ACIII serine 1076 mutated to alanine, or calmodulin-binding site on CNGB1b deleted. Crossing *Ano2*$^{-/-}$ with these animals will give the opportunity to directly examine the effect of these genetic modifications on CNG current kinetics.

Finally, we observed 'recovery translation invariance' in the olfactory responses, which was previously only seen and studied in photoreceptors. Further studies with mice that have components involved in transduction termination modified may provide understanding to the key termination step in olfactory transduction.

References

Adelson, E.H. (1982a). The delayed rod afterimage. Vision Res. *22*, 1313–1328.

Adelson, E.H. (1982b). Saturation and adaptation in the rod system. Vision Res. *22*, 1299–1312.

Allison, A.C. (1953). THE MORPHOLOGY OF THE OLFACTORY SYSTEM IN THE VERTEBRATES. Biol. Rev. *28*, 195–244.

Antolin, S., and Matthews, H.R. (2007). The effect of external sodium concentration on sodium-calcium exchange in frog olfactory receptor cells. J. Physiol. *581*, 495–503.

Antolin, S., Reisert, J., and Matthews, H.R. (2010). Olfactory response termination involves Ca2+-ATPase in vertebrate olfactory receptor neuron cilia. J. Gen. Physiol. *135*, 367–378.

Bakalyar, H. a, and Reed, R.R. (1990). Identification of a specialized adenylyl cyclase that may mediate odorant detection. Science *250*, 1403–1406.

Baylor, D.A., Hodgkin, A.L., and Lamb, T.D. (1974). The electrical response of turtle cones to flashes and steps of light. J. Physiol. *242*, 685–727.

Ben-Chaim, Y., Cheng, M.M., and Yau, K.-W. (2011). Unitary response of mouse olfactory receptor neurons. Proc. Natl. Acad. Sci. U. S. A. *108*, 822–827.

Bhandawat, V., Reisert, J., and Yau, K.-W. (2005). Elementary response of olfactory receptor neurons to odorants. Science *308*, 1931–1934.

Billig, G.M., Pál, B., Fidzinski, P., and Jentsch, T.J. (2011). Ca2+-activated Cl− currents are dispensable for olfaction. Nat. Neurosci. *14*, 763–769.

Boccaccio, A., and Menini, A. (2007). Temporal development of cyclic nucleotide-gated and Ca2+ -activated Cl- currents in isolated mouse olfactory sensory neurons. J. Neurophysiol. *98*, 153–160.

Boccaccio, A., Lagostena, L., Hagen, V., and Menini, A. (2006). Fast adaptation in mouse olfactory sensory neurons does not require the activity of phosphodiesterase. J. Gen. Physiol. *128*, 171–184.

Bönigk, W., Bradley, J., Müller, F., Sesti, F., Boekhoff, I., Ronnett, G. V, Kaupp, U.B., and Frings, S. (1999). The native rat olfactory cyclic nucleotide-gated channel is composed of three distinct subunits. J. Neurosci. *19*, 5332–5347.

Boschat, C., Pélofi, C., Randin, O., Roppolo, D., Lüscher, C., Broillet, M.-C., and Rodriguez, I. (2002). Pheromone detection mediated by a V1r vomeronasal receptor. Nat. Neurosci. *5*, 1261–1262.

Bozza, T., Feinstein, P., Zheng, C., and Mombaerts, P. (2002). Odorant receptor expression defines functional units in the mouse olfactory system. J. Neurosci. *22*, 3033–3043.

Bradley, J., Li, J., Davidson, N., Lester, H. a, and Zinn, K. (1994). Heteromeric olfactory cyclic nucleotide-gated channels: a subunit that confers increased sensitivity to cAMP. Proc. Natl. Acad. Sci. U. S. A. *91*, 8890–8894.

Bradley, J., Bönigk, W., Yau, K.-W., and Frings, S. (2004). Calmodulin permanently associates with rat olfactory CNG channels under native conditions. Nat. Neurosci. *7*, 705–710.

Bres, J., Bressolle, F., and Huguet, M. (1976). Importance de la dissociation ionique des médicaments en pharmacocinétique. Méthodes de détermination de leur pK a. Trav. Soc. Pharm. Montpellier *36*, 331–364.

Buck, L., and Axel, R. (1991). A novel multigene family may encode odorant receptors: a molecular basis for odor recognition. Cell *65*, 175–187.

Chess, A., Simon, I., Cedar, H., and Axel, R. (1994). Allelic inactivation regulates olfactory receptor gene expression. Cell *78*, 823–834.

Cygnar, K.D., and Zhao, H. (2009). Phosphodiesterase 1C is dispensable for rapid response termination of olfactory sensory neurons. Nat. Neurosci. *12*, 454–462.

Cygnar, K.D., Collins, S.E., Ferguson, C.H., Bodkin-Clarke, C., and Zhao, H. (2012). Phosphorylation of Adenylyl Cyclase III at Serine1076 Does Not Attenuate Olfactory Response in Mice. J. Neurosci. *32*, 14557–14562.

Dhallan, R.S., Yau, K.W., Schrader, K.A., and Reed, R.R. (1990). Primary structure and functional expression of a cyclic nucleotide-activated channel from olfactory neurons. Nature *347*, 184–187.

Ding, S., Wu, X., Li, G., Han, M., Zhuang, Y., and Xu, T. (2005). Efficient transposition of the piggyBac (PB) transposon in mammalian cells and mice. Cell *122*, 473–483.

Doving, K.B., and Trotier, D. (1998). Structure and function of the vomeronasal organ. J. Exp. Biol. *201*, 2913–2925.

Dzeja, C., Hagen, V., Kaupp, U.B., and Frings, S. (1999). Ca2+ permeation in cyclic nucleotide-gated channels. EMBO J. *18*, 131–144.

Firestein, S., and Werblin, F. (1989). Odor-induced membrane currents in vertebrate-olfactory receptor neurons. Science *244*, 79–82.

Fleischmann, A., Shykind, B.M., Sosulski, D.L., Franks, K.M., Glinka, M.E., Mei, D.F., Sun, Y., Kirkland, J., Mendelsohn, M., Albers, M.W., et al. (2008). Mice with a "Monoclonal Nose": Perturbations in an Olfactory Map Impair Odor Discrimination. Neuron *60*, 1068–1081.

Griff, E.R., Kleene, N.K., and Kleene, S.J. (2012). A selective PMCA inhibitor does not prolong the electroolfactogram in mouse. PLoS One *7*, e37148.

Hagino-Yamagishi, K., Matsuoka, M., Ichikawa, M., Wakabayashi, Y., Mori, Y., and Yazaki, K. (2001). The mouse putative pheromone receptor was specifically activated by stimulation with male mouse urine. J. Biochem. *129*, 509–512.

Hengl, T., Kaneko, H., Dauner, K., Vocke, K., Frings, S., and Möhrlen, F. (2010). Molecular components of signal amplification in olfactory sensory cilia. Proc. Natl. Acad. Sci. U. S. A. *107*, 6052–6057.

Hillenius, W.J., and Ruben, J.A. (2004). The evolution of endothermy in terrestrial vertebrates: Who? When? Why? Physiol. Biochem. Zool. *77*, 1019–1042.

Hu, H., Tian, J., Zhu, Y., Wang, C., Xiao, R., Herz, J.M., Wood, J.D., and Zhu, M.X. (2010). Activation of TRPA1 channels by fenamate nonsteroidal anti-inflammatory drugs. Pflugers Arch. *459*, 579–592.

Huang, F., Zhang, H., Wu, M., Yang, H., Kudo, M., Peters, C.J., Woodruff, P.G., Solberg, O.D., Donne, M.L., Huang, X., et al. (2012). Calcium-activated chloride channel TMEM16A modulates mucin secretion and airway smooth muscle contraction. Proc. Natl. Acad. Sci. *109*, 16354–16359.

Jaén, C., Ozdener, M.H., and Reisert, J. (2011). Mechanisms of chloride uptake in frog olfactory receptor neurons. J. Comp. Physiol. A Neuroethol. Sensory, Neural, Behav. Physiol. *197*, 339–349.

Jones, D.T., and Reed, R.R. (1989). Golf: an olfactory neuron specific-G protein involved in odorant signal transduction. Science *244*, 790–795.

Kaneko, H., Nakamura, T., and Lindemann, B. (2001). Noninvasive measurement of chloride concentration in rat olfactory receptor cells with use of a fluorescent dye. Am. J. Physiol. Cell Physiol. *280*, C1387–C1393.

Kaneko, H., Putzier, I., Frings, S., Kaupp, U.B., and Gensch, T. (2004). Chloride accumulation in mammalian olfactory sensory neurons. J. Neurosci. *24*, 7931–7938.

Kleene, S.J. (1993). Origin of the chloride current in olfactory transduction. Neuron *11*, 123–132.

Kleene, S.J. (1997). High-gain, low-noise amplification in olfactory transduction. Biophys. J. *73*, 1110–1117.

Kleene, S.J., and Gesteland, R.C. (1991). Calcium-activated chloride conductance in frog olfactory cilia. J. Neurosci. *11*, 3624–3629.

Kleene, S.J., Gesteland, R.C., and Bryant, S.H. (1994). An electrophysiological survey of frog olfactory cilia. J. Exp. Biol. *195*, 307–328.

Kuang, D., Yao, Y., Wang, M., Pattabiraman, N., Kotra, L.P., and Hampson, D.R. (2003). Molecular Similarities in the Ligand Binding Pockets of an Odorant Receptor and the Metabotropic Glutamate Receptors. J. Biol. Chem. *278*, 42551–42559.

Kucherenko, Y. V, and Lang, F. (2014). Niflumic acid affects store-operated Ca(2+)-permeable (SOC) and Ca (2+)-dependent K (+) and Cl (-) ion channels and induces apoptosis in K562 cells. J. Membr. Biol. *247*, 627–638.

Kurahashi, T. (1989). Activation by odorants of cation-selective conductance in the olfactory receptor cell isolated from the newt. J. Physiol.

Kurahashi, T. (1990). The response induced by intracellular cyclic AMP in isolated olfactory receptor cells of the newt. J. Physiol. *430*, 355–371.

Kurahashi, T., and Yau, K.W. (1993). Co-existence of cationic and chloride components in odorant-induced current of vertebrate olfactory receptor cells. Nature *363*, 71–74.

Leinders-Zufall, T., Lane, A.P., Puche, A.C., Ma, W., Novotny, M. V, Shipley, M.T., and Zufall, F. (2000). Ultrasensitive pheromone detection by mammalian vomeronasal neurons. Nature *405*, 792–796.

Leveteau, J., Andriason, I., Trotier, D., and MacLeod, P. (1989). Role of divalent cations in EOG generation. Chem. Senses *14*, 611–620.

Liman, E.R., and Buck, L.B. (1994). A second subunit of the olfactory cyclic nucleotide-gated channel confers high sensitivity to cAMP. Neuron *13*, 611–621.

Lowe, B.Y.G., and Gold, G.H. (1991). the Spatial Distributions of Odorant Sensitivity. 147–168.

Lowe, G., and Gold, G.H. (1993). Nonlinear amplification by calcium-dependent chloride channels in olfactory receptor cells. Nature *366*, 283–286.

Mombaerts, P. (2004). Genes and ligands for odorant, vomeronasal and taste receptors. Nat. Rev. Neurosci. *5*, 263–278.

Mombaerts, P., Wang, F., Dulac, C., Chao, S.K., Nemes, A., Mendelsohn, M., Edmondson, J., and Axel, R. (1996). Visualizing an olfactory sensory map. Cell *87*, 675–686.

Morrison, E.E., and Costanzo, R.M. (1990). Morphology of the human olfactory epithelium. J. Comp. Neurol. *297*, 1–13.

Morrison, E.E., and Costanzo, R.M. (1992). Morphology of olfactory epithelium in humans and other vertebrates. Microsc. Res. Tech. *23*, 49–61.

Nakamura, T., and Gold, G. (1987). A cyclic nucleotide-gated conductance in olfactory receptor cilia.

Nakashimo, Y., Takumida, M., Fukuiri, T., Anniko, M., and Hirakawa, K. (2010). Expression of transient receptor potential channel vanilloid (TRPV) 1–4, melastin (TRPM) 5 and 8, and ankyrin (TRPA1) in the normal and methimazole-treated mouse olfactory epithelium. Acta Otolaryngol. *130*, 1278–1286.

Nakatani, K., and Yau, K.W. (1988). Calcium and magnesium fluxes across the plasma membrane of the toad rod outer segment. J. Physiol. *395*, 695–729.

Ngai, J., Chess, A., Dowling, M.M., Necles, N., Macagno, E.R., and Axel, R. (1993). Coding of olfactory information: topography of odorant receptor expression in the catfish olfactory epithelium. Cell *72*, 667–680.

Nickell, W.T., Kleene, N.K., and Kleene, S.J. (2007). Mechanisms of neuronal chloride accumulation in intact mouse olfactory epithelium. J. Physiol. *583*, 1005–1020.

Nikonov, S., Engheta, N., and Pugh, E.N. (1998). Kinetics of recovery of the dark-adapted salamander rod photoresponse. J. Gen. Physiol. *111*, 7–37.

Pace, U., and Lancet, D. (1986). Olfactory GTP-binding protein: signal-transducing polypeptide of vertebrate chemosensory neurons. Proc. Natl. Acad. Sci. U. S. A. *83*, 4947–4951.

Pace, U., Hanski, E., Salomon, Y., and Lancet, D. (1985). Odorant-sensitive adenylate cyclase may mediate olfactory reception. Nature *316*, 255–258.

Pepperberg, D.R., Cornwall, M.C., Kahlert, M., Hofmann, K.P., Jin, J., Jones, G.J., and Ripps, H. (1992). Light-dependent delay in the falling phase of the retinal rod photoresponse. Vis. Neurosci. *8*, 9–18.

Pepperberg, D.R., Jin, J., and Jones, G.J. (1994). Modulation of transduction gain in light adaptation of retinal rods. Vis. Neurosci. *11*, 53–62.

Del Punta, K., Leinders-Zufall, T., Rodriguez, I., Jukam, D., Wysocki, C.J., Ogawa, S., Zufall, F., and Mombaerts, P. (2002). Deficient pheromone responses in mice lacking a cluster of vomeronasal receptor genes. Nature *419*, 70–74.

Reisert, J., and Matthews, H.R. (1998). Na+-dependent Ca2+ extrusion governs response recovery in frog olfactory receptor cells. J. Gen. Physiol. *112*, 529–535.

Reisert, J., Bauer, P.J., Yau, K.-W., and Frings, S. (2003). The Ca-activated Cl channel and its control in rat olfactory receptor neurons. J. Gen. Physiol. *122*, 349–363.

Reisert, J., Lai, J., Yau, K.-W., and Bradley, J. (2005). Mechanism of the excitatory Cl- response in mouse olfactory receptor neurons. Neuron *45*, 553–561.

Ressler, K.J., Sullivan, S.L., and Buck, L.B. (1993). A zonal organization of odorant receptor gene expression in the olfactory epithelium. Cell *73*, 597–609.

Restrepo, D., Miyamoto, T., Bryant, B.P., and Teeter, J.H. (1990). Odor stimuli trigger influx of calcium into olfactory neurons of the channel catfish. Science *249*, 1166–1168.

Rodriguez, I. (2004). Pheromone receptors in mammals. Horm. Behav. *46*, 219–230.

Sagheddu, C., Boccaccio, A., Dibattista, M., Montani, G., Tirindelli, R., and Menini, A. (2010a). Calcium concentration jumps reveal dynamic ion selectivity of calcium-activated chloride currents in mouse olfactory sensory neurons and TMEM16b-transfected HEK 293T cells. J. Physiol. *588*, 4189–4204.

Sagheddu, C., Boccaccio, A., Dibattista, M., Montani, G., Tirindelli, R., and Menini, A. (2010b). Calcium concentration jumps reveal dynamic ion selectivity of calcium-activated chloride currents in mouse olfactory sensory neurons and TMEM16b-transfected HEK 293T cells. J. Physiol. *588*, 4189–4204.

Sato, T., Hirono, J., Tonoike, M., and Takebayashi, M. (1991). Two types of increases in free Ca2+ evoked by odor in isolated frog olfactory receptor neurons. Neuroreport *2*, 229–232.

Sklar, P. (1987). The Odorant-Sensitive Adenylate Cyclase of Olfactory Receptor Cells. … New York Acad. … 15538–15543.

Song, Y., Cygnar, K.D., Sagdullaev, B., Valley, M., Hirsh, S., Stephan, A., Reisert, J., and Zhao, H. (2008). Olfactory CNG Channel Desensitization by Ca2+/CaM via the B1b Subunit Affects Response Termination but Not Sensitivity to Recurring Stimulation. Neuron *58*, 374–386.

Stephan, A.B., Shum, E.Y., Hirsh, S., Cygnar, K.D., Reisert, J., and Zhao, H. (2009). ANO2 is the cilial calcium-activated chloride channel that may mediate olfactory amplification. Proc. Natl. Acad. Sci. U. S. A. *106*, 11776–11781.

Stephan, A.B., Tobochnik, S., Dibattista, M., Wall, C.M., Reisert, J., and Zhao, H. (2011). The Na+/Ca2+ exchanger NCKX4 governs termination and adaptation of the mammalian olfactory response. Nat. Neurosci. *15*, 131–137.

Thuret, S., Moon, L.D.F., and Gage, F.H. (2006). Therapeutic interventions after spinal cord injury. Nat. Rev. Neurosci. *7*, 628–643.

Vassar, R., Ngai, J., and Axel, R. (1993). Spatial segregation of odorant receptor expression in the mammalian olfactory epithelium. Cell *74*, 309–318.

Vassar, R., Chao, S.K., Sitcheran, R., Nuñez, J.M., Vosshall, L.B., and Axel, R. (1994). Topographic organization of sensory projections to the olfactory bulb. Cell *79*, 981–991.

Vocke, K., Dauner, K., Hahn, A., Ulbrich, A., Broecker, J., Keller, S., Frings, S., and Möhrlen, F. (2013). Calmodulin-dependent activation and inactivation of anoctamin calcium-gated chloride channels. J. Gen. Physiol. *142*, 381–404.

Wayman, G.A., Impey, S., and Storm, D.R. (1995). Ca2+ inhibition of type III adenylyl cyclase in vivo. J. Biol. Chem. *270*, 21480–21486.

Wei, J., Wayman, G., and Storm, D.R. (1996). Phosphorylation and inhibition of type III adenylyl cyclase by calmodulin-dependent protein kinase II in vivo. J. Biol. Chem. *271*, 24231–24235.

Yan, C., Zhao, a Z., Bentley, J.K., Loughney, K., Ferguson, K., and Beavo, J. a (1995). Molecular cloning and characterization of a calmodulin-dependent phosphodiesterase enriched in olfactory sensory neurons. Proc. Natl. Acad. Sci. U. S. A. *92*, 9677–9681.

Yau, K.-W., and Nakatani, K. (1984a). Cation selectivity of light-sensitive conductance in retinal rods. Nature *309*, 352–354.

Yau, K.-W., and Nakatani, K. (1984b). Electrogenic Na–Ca exchange in retinal rod outer segment. Nature *311*, 661–663.

Curriculum Vitae

Chih-Chun LIN June 11. 2015

Educational History

Ph.D. expected	2015	Department of Neuroscience, Johns Hopkins School of Medicine Advisor: King-Wai YAU Ph.D.
M.D.	2004	School of Medicine, National Taiwan University

Other professional experience

Neurology resident	2004-2008	Department of neurology, National Taiwan University Hospital
Senior clerkship	2003	School of Medicine, Northwestern University
Research assistant	2001	Lab of Morgan Sheng, Massachusetts Institute of Technology
Research assistant	2000	Lab of Li-Chu Chou and Chanley Young, National Taiwan University

Scholarship and fellowship

Scholarship for overseas graduate study, Ministry of Education, Taiwan 2008

Academic honors

2004	Best intern of the year
2004	Best intern of internal medicine
1997-2000	Presidential awards
1997	Silver medal, International Physics Olympiad

Publications, peer-reviewed

Chen TF*, **Lin CC***, Chen YF, Liu HM, Hua MS, Huang YC, Chiu MJ. Diffusion tensor changes in patients with amnesic mild cognitive impairment and various dementias. *Psychiatry Res*. 2009 Jul 15; 173(1):15-21 ***Equal contribution**

Lin CC, Chiu MJ. Cervical cord atrophy with sensory ganglionopathy in Sjogren syndrome. *Neurology,* 2008 Feb 12; 70(7):e27.

Hering H, **Lin CC**, Sheng M.Cholesterol/sphingolipid rafts in the maintenance of synapses, dendritic spines, and surface AMPA receptor stability. *Journal of Neuroscience*, 2003 Apr 15; 23(8): 3262-71.

Service and leadership

2009 Teaching assistant, Neuroscience and Cognition I. Department of Neuroscience, Johns Hopkins School of Medicine